


ARTICLE

Nek2-mediated GAS2L1 phosphorylation and centrosome-linker disassembly induce centrosome disjunction

Franco K.C. Au^{1,2}, Bill K.T. Hau^{1,2}, and Robert Z. Qi^{1,2} 

Centrosome disjunction occurs in late G2 to facilitate bipolar spindle formation and is mediated by the NIMA-related kinase Nek2. Here, we show that GAS2L1, a microtubule- and F-actin-binding protein required for centrosome disjunction, undergoes Nek2-mediated phosphorylation at Ser352 in G2/M. The phosphorylation is essential for centrosome disjunction in late G2 and for proper spindle assembly and faithful chromosome segregation in mitosis. GAS2L1 contains a calponin-homology (CH) domain and a GAS2-related (GAR) domain, which bind to F-actin and microtubules, respectively. Notably, the CH and GAR domains bind to each other to inhibit the functions of both domains, and Ser352 phosphorylation disrupts the interaction between the two domains and relieves the autoinhibition. We dissected the roles of the GAS2L1 phosphorylation and of centrosome-linker disassembly, which is another Nek2-mediated event, and found that these events together trigger centrosome disjunction. Therefore, our findings demonstrate the concerted Nek2 actions that split the centrosomes in late G2.

Introduction

Precise chromosome segregation in mitosis requires the assembly of a bipolar spindle apparatus, which contains a centrosome at each spindle pole for organizing spindle microtubules. The centrosome, which comprises a pair of centrioles embedded in pericentriolar material (PCM), duplicates once per cell division cycle, and before mitotic entry, the two duplicated centrosomes are separated to prepare them for the formation of the spindle poles during mitosis. During mitosis, the mother and daughter centrioles of each centrosome are disengaged (Nigg and Stearns, 2011). At the end of mitosis, both daughter cells therefore inherit, in addition to an equal number of chromosomes, a centrosome harboring the disengaged centrioles. From mitotic exit to late G2, the disengaged centrioles and subsequently the two duplicated centrosomes are held together by the centrosome linker, whose major component is rootletin assembled into a network that is tethered by C-Nap1 to the proximal end of centrioles (Bahe et al., 2005; Yang et al., 2006; Graser et al., 2007; He et al., 2013; Fang et al., 2014; Vlijm et al., 2018).

The initiation of centrosome separation, which occurs in late G2 and is frequently referred to as centrosome disjunction, is marked by centrosome-linker disassembly (Faragher and Fry, 2003; Mardin et al., 2010, 2011). After disjunction, the centrosomes move apart in

mitosis to the two opposite sides of the cell; this process is mainly driven by the microtubule motor Eg5 (kinesin-5), which slides apart the antiparallel microtubules and therefore creates forces for further separation of the centrosomes (Sawin et al., 1992; Blangy et al., 1995; Smith et al., 2011), and this centrosome movement is also facilitated by kinetochore-generated forces after nuclear envelope breakdown (NEBD; Toso et al., 2009; McHedlishvili et al., 2012). During the cell cycle, centrosome disjunction, which occurs before mitotic entry, is required for proper mitosis because it ensures the precise timing of centrosome separation (Mardin et al., 2010; Kaseda et al., 2012; Silkworth et al., 2012).

Centrosome-linker disassembly results from the phosphorylation of rootletin and several other linker proteins by NIMA-related kinase 2A (Nek2A), which is accumulated on centrosomes in G2/M through the Plk1-Mst2/hSav pathway and initiates centrosome separation (Faragher and Fry, 2003; Rellos et al., 2007; Mardin et al., 2010, 2011). Nek2A overexpression was found to cause premature separation of centrosomes, whereas overexpression of a kinase-dead Nek2A mutant or RNAi-mediated depletion of Nek2A inhibited the disjunction in late G2 (Fry et al., 1998b; Faragher and Fry, 2003; Fletcher et al., 2005; Mardin et al., 2010). Therefore, Nek2A plays a key role in inducing the disjunction.

¹Division of Life Science and State Key Laboratory of Molecular Neuroscience, The Hong Kong University of Science and Technology, Hong Kong, China; ²Shenzhen Key Laboratory of Edible and Medicinal Bioresources, HKUST Shenzhen Research Institute, Shenzhen, China.

Correspondence to Robert Z. Qi: qirz@ust.hk.

© 2020 Au et al. This article is distributed under the terms of an Attribution–Noncommercial–Share Alike–No Mirror Sites license for the first six months after the publication date (see <http://www.rupress.org/terms/>). After six months it is available under a Creative Commons License (Attribution–Noncommercial–Share Alike 4.0 International license, as described at <https://creativecommons.org/licenses/by-nc-sa/4.0/>).

Nek2B and Nek2C are two splice variants of Nek2A: Nek2B lacks a carboxy-terminal coiled-coil region and is dispensable for centrosome disjunction (Uto and Sagata, 2000; Fletcher et al., 2005); conversely, Nek2C is identical to Nek2A except that it lacks aa 371–378, and Nek2C exhibits biochemical features almost indistinguishable from those of Nek2A (Naro et al., 2014). However, Nek2C expression was reported to be barely detectable in various mammalian cell lines examined (Naro et al., 2014).

Recently, we demonstrated that growth-arrest-specific 2 (GAS2)-like 1 (GAS2L1) functions in centrosome motility and disjunction by attaching F-actin and microtubules to the proximal end of mature centrioles (Au et al., 2017). Actin filaments and microtubules have been known to participate in centrosome disjunction, and both are considered to exert pulling and pushing forces on centrosomes (Uzbekov et al., 2002; Burakov et al., 2003; Wang et al., 2008; Cao et al., 2010; Kimura and Kimura, 2011; Vaughan and Dawe, 2011; Agircan et al., 2014; Obino et al., 2016). GAS2L1, a member of the GAS2 family, harbors a calponin-homology (CH) domain followed by a GAS2-related (GAR) domain at the amino-terminal region and contains a Ser-x-Ile-Pro (SxIP; x represents any amino acid) motif near the carboxy terminus (Goriounov et al., 2003; Jiang et al., 2012). The CH and GAR domains exhibit F-actin- and microtubule-binding activity, respectively, and the SxIP motif is for binding to End-binding proteins (EBs); these activities are all involved in the centrosome-separating function of GAS2L1 (Au et al., 2017). GAS2L1 overexpression promotes centrosome disjunction, an effect that can be counteracted by strengthening the centrosome linker. Therefore, centrosome disjunction occurs if forces exerted from the GAS2L1-attached cytoskeletons cannot be counterbalanced by the centrosome linker (Au et al., 2017).

It is unknown whether and how GAS2L1 is regulated for centrosome disjunction. As a first step in answering these questions, we report here that GAS2L1 is hyperphosphorylated in G2/M, coincident with the onset of centrosome disjunction, and we identify the residues that undergo drastically increased phosphorylation in mitosis. Our mutational analysis revealed that Ser352 phosphorylation is essential for the centrosome-separating activity of GAS2L1 and for proper spindle assembly and chromosome segregation. Notably, we found that within GAS2L1, the CH and GAR domains exert an autoinhibitory effect on each other and that Ser352 phosphorylation relieves the autoinhibition. We also show that Ser352 phosphorylation is induced in G2/M and catalyzed by Nek2A. Thus, Nek2A mediates GAS2L1 activation in addition to centrosome-linker disassembly, and these two actions together drive centrosome disjunction.

Results

Centrosome disjunction requires GAS2L1 phosphorylation at Ser352

Because centrosome disjunction is a cell cycle stage-specific event, we reasoned that GAS2L1 activity is likely controlled tightly. Thus, to first monitor GAS2L1 expression during the cell cycle, we synchronized HeLa cells by double-thymidine treatment and then released the cells from the G1/S arrest. At ~12 h

post-release, the cells progressed into mitosis, as shown by the expression of cyclin B1 (Fig. 1 A). During the cell cycle progression from G1/S to mitosis, GAS2L1 protein level did not change markedly (Fig. 1 A). Intriguingly, however, the GAS2L1 band from mitotic cells showed an upshift, and this upshift was eliminated by phosphatase treatment of the mitotic cell extracts (Fig. 1, A and B). These observations indicated mitotic phosphorylation of GAS2L1.

To identify the cell cycle-dependent phosphorylation of GAS2L1, a stable cell line expressing GFP-GAS2L1 was synchronized to interphase or mitosis, and GAS2L1 was immunoprecipitated from the cells and analyzed using mass spectrometry (Fig. 1 C, left). In accord with the aforementioned data, GAS2L1 from nocodazole-arrested mitotic cells showed an upshift in SDS-PAGE mobility (Fig. 1 C, right). By comparing the mass-spectrometric results of interphase and mitotic GAS2L1, we found that GAS2L1 phosphorylation was drastically induced at 12 residues, with 5 of the residues being clustered in the short region aa 352–360 (Ser352, Ser355, Ser357, Ser358, and Ser360; Fig. 1 D). Most of these five serines and the surrounding sequence are conserved in GAS2L1 vertebrate homologues (Fig. 1 E).

We investigated the function of the phosphorylation of the clustered serines by replacing all five Ser residues with either Asp to create a phosphomimetic mutant (5D) or Ala to create a non-phosphorylatable mutant (5A), and we transiently expressed the mutant and WT constructs in cells. Overexpression of WT GAS2L1 induced centrosome separation ($d > 2 \mu\text{m}$ in ~62% of transfected cells; hereafter, d represents intercentrosome distance; Fig. 2 A), which agrees with our previous report (Au et al., 2017). By comparison, cells expressing the 5A mutant exhibited drastically attenuated centrosome-splitting activity ($d > 2 \mu\text{m}$ in ~37% of 5A-transfected cells), but cells expressing the 5D mutant effectively split the centrosomes ($d > 2 \mu\text{m}$ in ~66% of 5D-transfected cells; Fig. 2 A). Next, we mutated the five Ser residues individually to Asp or Ala. The S352D single mutant showed strong centrosome-splitting activity, which was similar to that measured with the 5D mutant ($d > 2 \mu\text{m}$ in ~64% of S352D-transfected cells), whereas with the S352A mutant, centrosome-splitting activity was lowered to the same extent in the case of the 5A mutant ($d > 2 \mu\text{m}$ in ~39% of S352A-transfected cells; Fig. 2 A). By contrast, single mutations of the remaining four serines did not produce any notable effect on centrosome-splitting activity (Fig. S1).

To demonstrate that GAS2L1 function does not depend on phosphorylation at Ser355, Ser357, Ser358, and Ser360 but requires Ser352 phosphorylation, we created the mutant S352A/4D, in which Ser355, Ser357, Ser358, and Ser360 were mutated to Asp and Ser352 was mutated to Ala. S352A/4D showed markedly diminished centrosome-splitting activity ($d > 2 \mu\text{m}$ in ~36% of transfected cells), which was as low as the activity of the 5A and S352A mutants (Fig. 2 A). Similarly, we generated the mutant S352D/4A, in which Ser352 was mutated to Asp and Ser355, Ser357, Ser358, and Ser360 were mutated to Ala, and we found that in cells transfected with S352D/4A, centrosome separation occurred as effectively as in cells transfected with the 5D or S352D mutant ($d > 2 \mu\text{m}$ in ~66% of transfected cells; Fig. 2 A). Collectively, the findings of these mutational analyses indicate that Ser352 phosphorylation is required for stimulating the

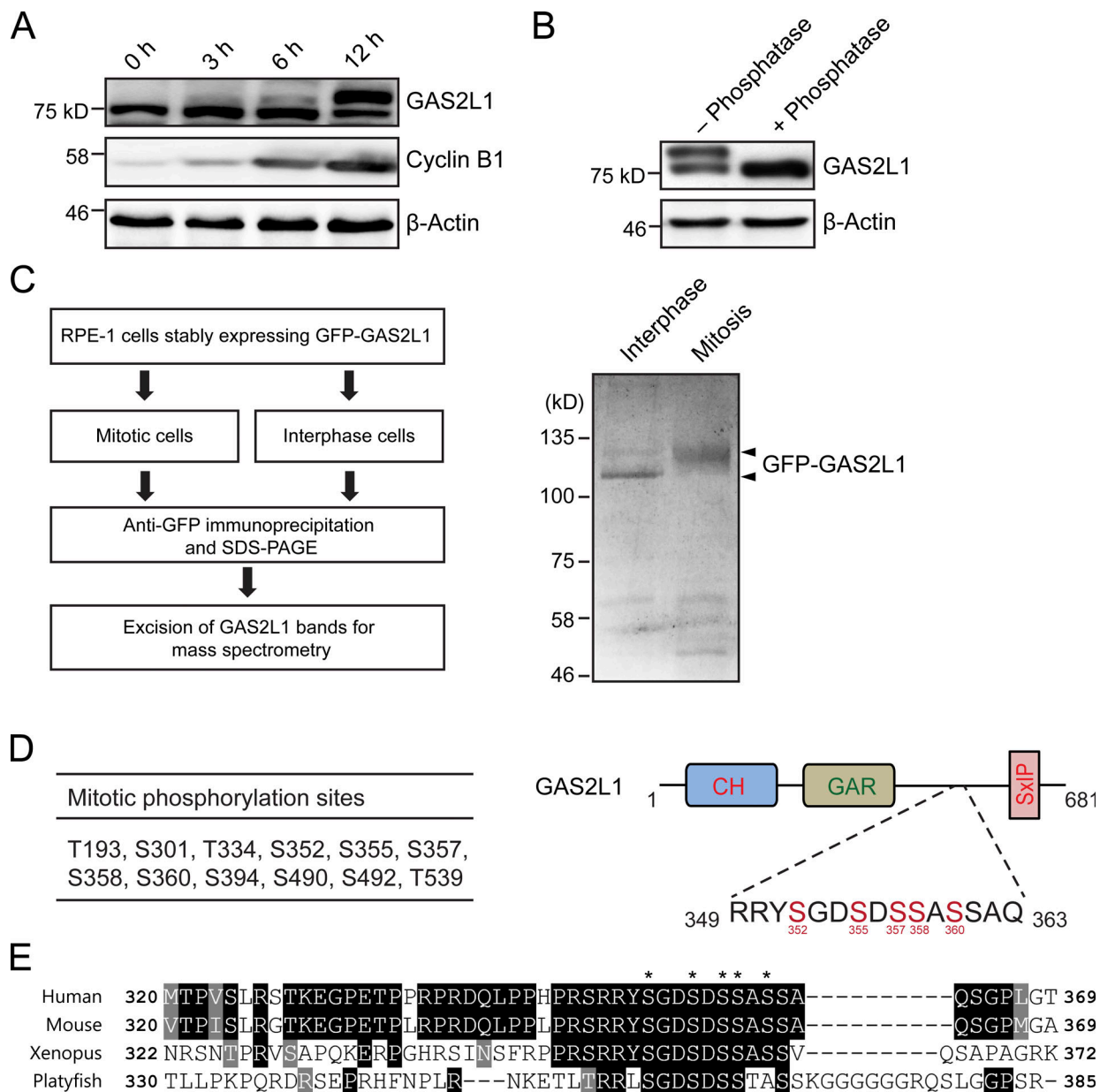


Figure 1. GAS2L1 undergoes cell cycle-dependent phosphorylation. (A) HeLa cells were released from double-thymidine block into medium containing 5 μ M STLIC. Whole-cell extracts were collected at indicated times and immunoblotted with antibodies against GAS2L1, cyclin B1, and β -actin. (B) Following double-thymidine release for 12 h, HeLa cells were lysed and incubated at 30°C with or without calf intestinal alkaline phosphatase for 15 min; subsequently, cell extracts were immunoblotted with antibodies against GAS2L1 and β -actin. (C) Left: Preparation of GAS2L1 samples for identification of phosphorylation sites by using mass spectrometry. Right: Coomassie Blue–stained gel of GAS2L1 proteins immunoprecipitated (using the attached tag) from interphase and mitotic cells. (D) Left: GAS2L1 residues identified to undergo mitotically induced phosphorylation. Right: Schematic structure of GAS2L1 indicating the location of five clustered Ser-phosphorylation sites. (E) Sequence alignment of GAS2L1 from various vertebrate species. Asterisks: identified phosphorylation sites within the region.

centrosome-separating activity of GAS2L1, but that phosphorylation of the other residues is dispensable.

To further evaluate the role of GAS2L1 phosphorylation in its physiological functions, we generated a *gas2li*-knockout line of hTERT RPE-1 (RPE-1) cells and stably expressed WT GAS2L1 or the mutants S352A and S352D in the *gas2li*^{-/-} cells at levels close to that of endogenous GAS2L1 in parental RPE-1 cells (Fig. 2 B). The GAS2L1-null cells and the stable-expression sublines did not exhibit any overt defect in cell growth, but the *gas2li*^{-/-} cells

showed clear defects in centrosome disjunction: only ~22% of the G2 cells, which were identified based on positive staining for Centromere protein F (CENP-F), contained split centrosomes ($d > 2 \mu$ m), as compared with ~53% of the G2 cells of the parental RPE-1 line (Fig. 2 C). These results support our previous results obtained from RNAi-mediated silencing of GAS2L1 expression (Au et al., 2017).

In the *gas2li*^{-/-} cells, low-level ectopic expression of GAS2L1 restored centrosome separation to the same extent as in the

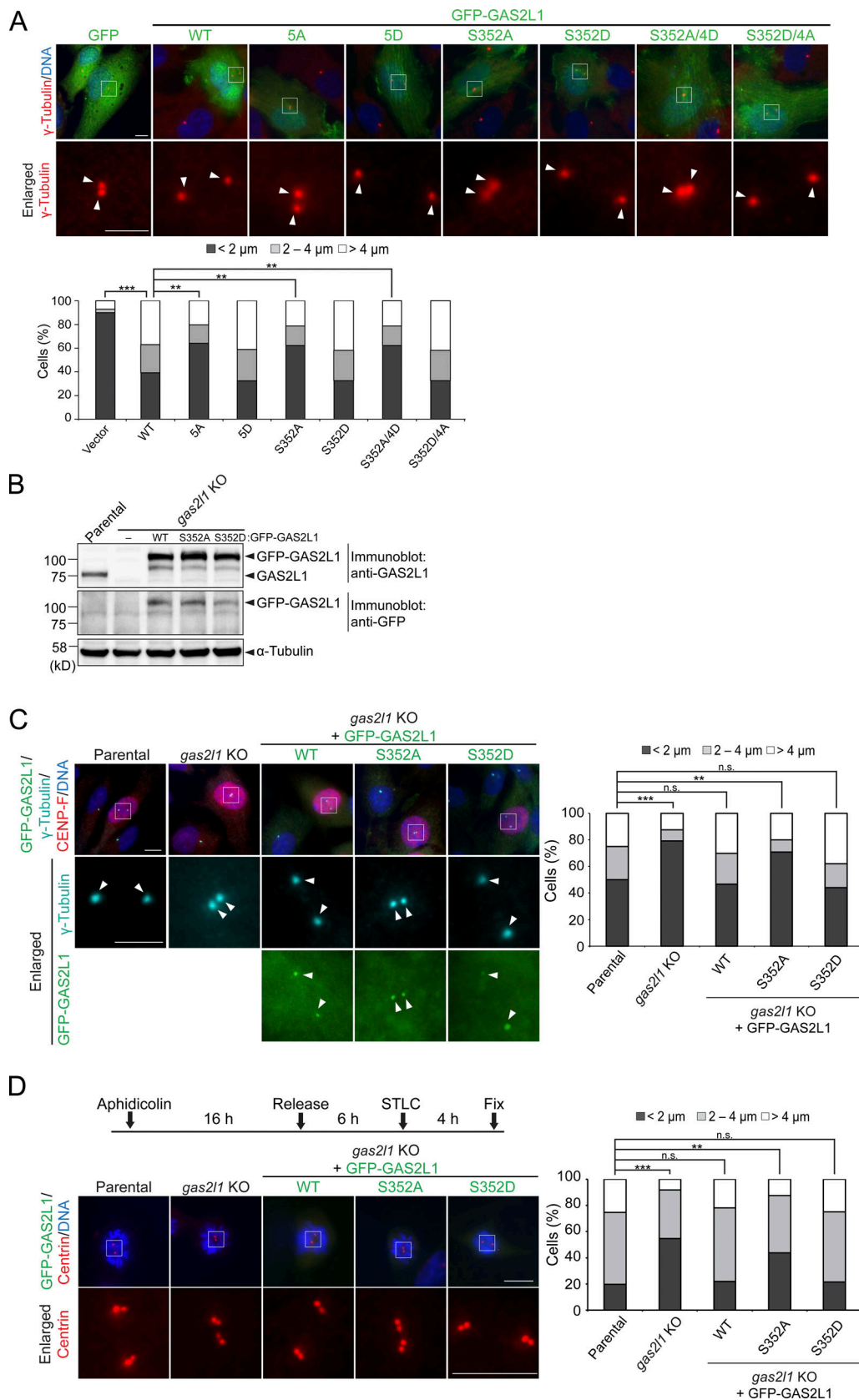


Figure 2. **Phosphorylation at Ser352 is required for GAS2L1 function in centrosome separation.** (A) Asynchronous RPE-1 cells were transfected with GFP or the following GFP-tagged GAS2L1 constructs: WT and mutants 5A, 5D, S352A, S352D, S352A/4D, and S352D/4A. Centrosomes were labeled with anti- γ -tubulin antibody. Centrosome distance was measured in the transfected cells from three independent experiments: $n = 96$ (GFP), 110 (WT), 120 (5A), 114 (5D),

112 (S352A), 110 (S352D), 100 (S352A/4D), and 100 (S352D/4A). Arrowheads: centrosomes. **(B)** GAS2L1 expression was examined in RPE-1 parental cells and sublines. *gas2l1* KO, *gas2l1*-knockout line; GFP-GAS2L1 (WT) or mutants (S352A and S352D) were stably expressed in the knockout line. Anti-GAS2L1, anti-GFP, and anti- α -tubulin immunoblotting was performed. **(C)** RPE-1 parental cells and sublines were stained for CENP-F and γ -tubulin. Centrosome distance during late G2 was measured from CENP-F-positive cells in three independent experiments: $n = 161$ (parental), 170 (*gas2l1* KO), 150 (WT), 162 (S352A), and 149 (S352D). Arrowheads: centrosomes. **(D)** RPE-1 lines as in C were arrested with aphidicolin and then released and treated with STLC. Centrosomes were labeled through anti-centrin staining. Centrosome distance was measured in mitotic cells (arrested in prometaphase by STLC) from three independent experiments: $n = 100$ (parental), 100 (*gas2l1* KO), 120 (WT), 123 (S352A), and 121 (S352D). **(A, C, and D)** Arrowheads, centrosomes. Scale bars, 10 μm in cell micrographs and 5 μm in enlarged images. χ^2 test; **, $P < 0.001$; ***, $P < 0.0001$; n.s., not significant.

parental RPE-1 line (Fig. 2 C). Moreover, expression of the S352D mutant produced a similar rescue effect as expression of the WT protein, whereas S352A expression did not rescue the disjunction defect (Fig. 2 C). To verify that the centrosome disjunction triggered by Ser352 phosphorylation of GAS2L1 is independent of Eg5, we treated cells with the Eg5 inhibitor S-trityl-L-cysteine (STLC) and then measured intercentrosome distances in the mitotic cells of the GAS2L1-null line and the stable expression sublines: expression of WT or S352D restored centrosome disjunction but that of S352A did not (Fig. 2 D), and these effects were similar to those observed in rescue experiments conducted without STLC treatment (Fig. 2 C). These results and the results of the aforementioned rescue experiments corroborate those of the transient overexpression assays (Fig. 2 A) in terms of the requirement of Ser352 phosphorylation for GAS2L1 function in centrosome separation. Our results further indicate that this GAS2L1 function does not involve the action of Eg5.

GAS2L1 and its Ser352 phosphorylation are necessary for error-free mitosis

Timely centrosome separation before mitotic entry and the subsequent Eg5-driven poleward movement of the centrosomes represent a well-coordinated process that facilitates spindle formation, mitotic progression, and chromosome segregation (Kaseda et al., 2012; Silkworth et al., 2012; Mardin et al., 2013; Nam and van Deursen, 2014). We performed time-lapse imaging through G2 and mitosis on parental and *gas2l1*^{-/-} RPE-1 cells as well as *gas2l1*^{-/-} cells expressing WT GAS2L1 and the Ser352 mutants. In early G2, all five cell lines showed similar intercentrosomal distances, of 1–2 μm , with small oscillatory intercentrosomal movements (Fig. 3, A and B; and Videos 1, 2, 3, 4, and 5). Centrosome disjunction ($d > 2 \mu\text{m}$) occurred at markedly later times in *gas2l1*^{-/-} cells and S352A-expressing *gas2l1*^{-/-} cells (~39 and ~44 min before NEBD, respectively) than in the parental cells (~72 min before NEBD; Fig. 3, A–C; and Videos 1, 2, and 4), whereas the disjunction occurred at, respectively, ~77 and ~75 min before NEBD in *gas2l1*^{-/-} cells expressing WT and S352D GAS2L1 (Fig. 3, A–C; and Videos 3 and 5). Disjunction might have occurred slightly earlier in the cells rescued with WT and S352D GAS2L1 due to the exogenous proteins being expressed at slightly higher levels than endogenous GAS2L1 in the parental cells (Fig. 2 B).

We evaluated the effect of *gas2l1* knockout and the disruption of Ser352 phosphorylation on mitotic progression. As compared with parental cells, *gas2l1*^{-/-} cells showed an increase in mitosis length of ~8 min (Fig. 3 D). Reexpression of WT or S352D GAS2L1 restored mitosis length to that in the parental cells, whereas S352A expression did not notably shorten the prolonged mitosis (Fig. 3 D).

Similar observations were obtained when we measured metaphase durations (Fig. 3 D). Prometaphase and anaphase were unaffected by *gas2l1* knockout or the reexpression of the Ser352 mutants (Fig. 3 D). However, we observed chromosome bridges in anaphase *gas2l1*^{-/-} cells and S352A-expressing *gas2l1*^{-/-} cells (Fig. 3 A). Altogether, our data strongly suggest that the delay of centrosome disjunction caused by *gas2l1* knockout or the disruption of GAS2L1 Ser352 phosphorylation specifically affects metaphase. This is also supported by the previous observation that premature centrosome separation shortens metaphase (Mardin et al., 2013).

We tested whether GAS2L1 and its Ser352 phosphorylation are involved in mitotic spindle assembly. In metaphase *gas2l1*^{-/-} cells, a bipolar spindle frequently formed with altered geometry: the pole-to-pole spindle axis was not oriented perpendicular to the metaphase plate (Fig. 4 A). Measurement of the angle of the spindle axis to the long axis of the metaphase plate revealed that in control RPE-1 cells, the mean value was 87.4° (Fig. 4 A), which is similar to that reported previously (Prosser et al., 2015). The mean value dropped to ~84.4° in *gas2l1*^{-/-} cells (Fig. 4 A), but, notably, was restored to 87.4° and 87.5° following reexpression of WT and S352D GAS2L1, respectively; by contrast, the angle remained at 83.8° after S352A expression (Fig. 4 A). Therefore, S352A expression did not rescue the spindle geometry defect.

Metaphase cells displaying altered spindle geometry tend to exhibit errors in chromosome segregation (Silkworth and Cimini, 2012). We also observed that the incidence of chromosome segregation defects, such as chromosome bridges and lagging chromosomes, was higher in anaphase *gas2l1*^{-/-} cells than parental RPE-1 cells (~18% and ~5%, respectively; Fig. 3 A and Fig. 4 B). The incidence of the defects was lowered almost to the level in parental cells after the expression of WT GAS2L1 or S352D in *gas2l1*^{-/-} cells (~4% and ~5%, respectively; Fig. 3 A and Fig. 4 B), but S352A expression did not produce this rescue effect (~16% for S352A-expressing cells; Fig. 4 B). Furthermore, in *gas2l1*^{-/-} and S352A-rescued cells, the incidence of chromosome mis-segregation closely correlated with the delay of centrosome disjunction: in the cells exhibiting chromosome segregation errors, centrosome disjunction was delayed by ~24 min on average (Fig. 4 C). Therefore, Ser352 phosphorylation is indispensable for GAS2L1 function in spindle assembly and chromosome segregation.

To exclude the possibility that *gas2l1* knockout or the rescue by S352A expression causes PCM abnormalities, which could lead to mitotic errors (Lane and Nigg, 1996; Lee and Rhee, 2011; Joukov et al., 2014), we examined the centrosomal localization of γ -tubulin, a core component of microtubule nucleator γ -tubulin ring complexes; we found that neither *gas2l1* knockout nor the rescue with S352A or S352D mutant affected γ -tubulin localization on interphase and mitotic centrosomes (Fig. 4 A and Fig.

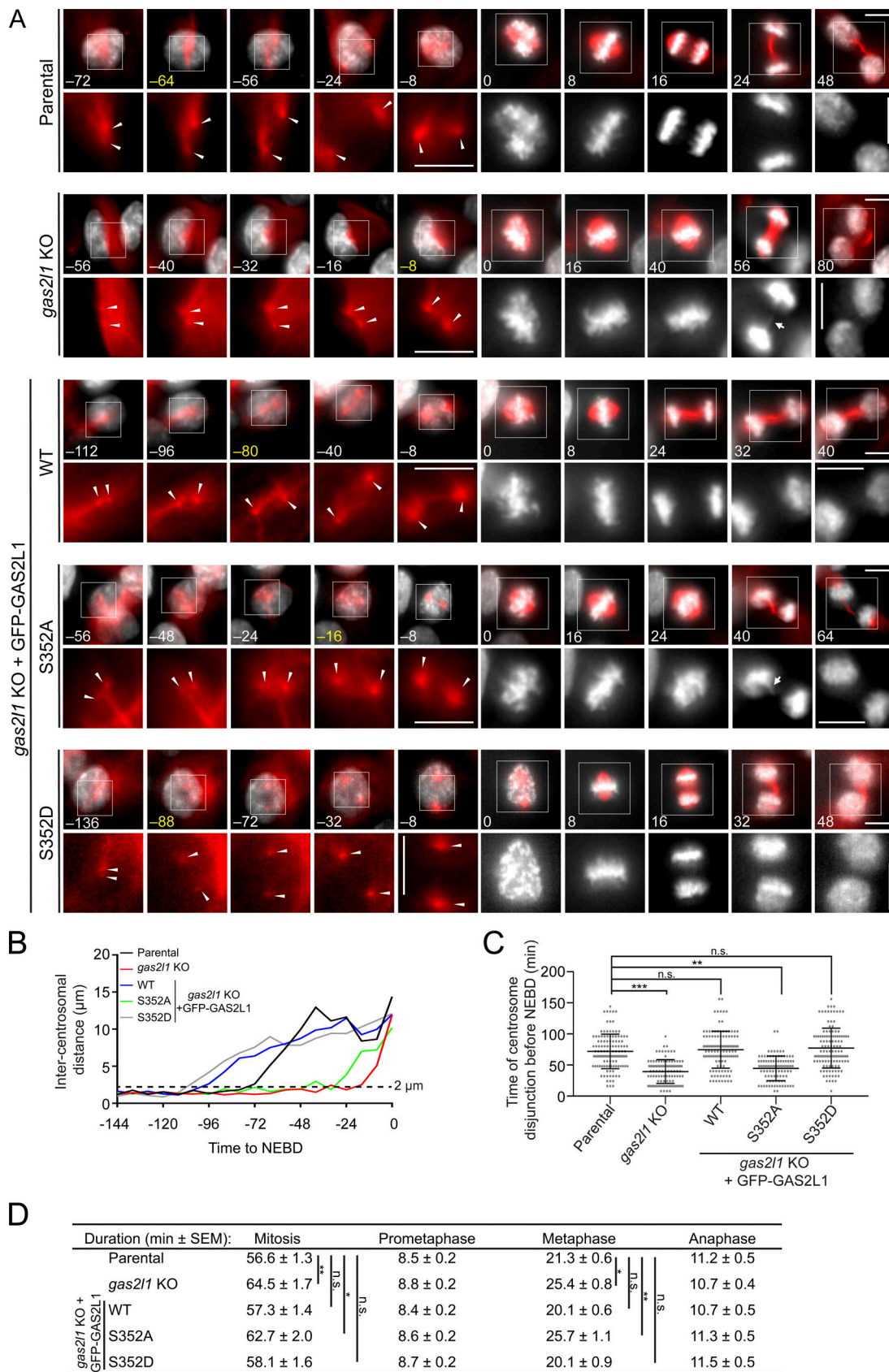


Figure 3. **GAS2L1 and its Ser352 phosphorylation regulate centrosome separation and facilitate mitotic progression.** (A) Representative time-lapse sequences of parental RPE-1 cells and the indicated sublines before and during mitosis. Images are labeled with times relative to NEBD; $t = 0$, time of NEBD; onset times of centrosome disjunction are shown in yellow. Boxed areas are enlarged. Arrowheads: centrosomes; arrows in *gas2l1*^{-/-} cells and S352A-

expressing *gas2l1*^{-/-} cells: chromosome bridges. Scale bar, 5 μ m. **(B)** Intercentrosomal distances measured before NEBD from cells in A; $t = 0$, time of NEBD. **(C)** Dot plot of times of centrosome disjunction ($d > 2 \mu$ m) occurrence. Each dot represents a single cell with data collected. Midline: mean; upper and lower lines: SD. **(D)** Durations of mitosis and different mitotic stages presented as means \pm SEM. **(C and D)** Data were quantified from three different experiments: $n = 122$ (parental), 107 (*gas2l1* KO), 118 (WT), 96 (S352A), and 121 (S352D). One-way ANOVA; *, $P < 0.01$; **, $P < 0.001$; ***, $P < 0.0001$; n.s., not significant.

S2 A). This agrees with the results we obtained following RNAi-mediated suppression of GAS2L1 expression (Au et al., 2017). Similarly, the centrosomal content of the PCM scaffold protein pericentrin was unaltered by the knockout and the mutant rescues (Fig. S2 B and data not shown). Centrosome maturation occurs in late G2 and mitosis and is characterized by PCM expansion and increased microtubule-nucleating activity (Palazzo et al., 2000). The knockout and the mutant rescues did not affect PCM expansion (Fig. S2, A and B) or centrosome-based microtubule regrowth in G2/M cells (Fig. S2 C). These observations indicate that centrosome maturation is unperturbed by the disruption of GAS2L1 expression or Ser352 phosphorylation.

GAS2L1 function is regulated by autoinhibition

To gain mechanistic insights into the effect of Ser352 phosphorylation, we further characterized the functional properties of GAS2L1 and prepared a series of GAS2L1 fragments for assays (Fig. 5 A). First, we assessed the association of F-actin with GAS2L1 fragments and the intact protein. GAS2L1 and its fragments transiently expressed in cells were immunoprecipitated through the ectopic tag, and the coimmunoprecipitation of actin was examined. In agreement with a previous report (Goriounov et al., 2003), the CH domain displayed robust actin-binding activity (Fig. 5 B), and deletion of this domain eliminated the actin-binding activity of GAS2L1 (GAR-Tail; Fig. 5 B). Therefore, we conclude that the CH domain is responsible for the actin-binding function. Intriguingly, actin binding of intact GAS2L1 was considerably weaker than that of the CH-only fragment, and deletion of the GAR domain drastically increased the actin-binding activity of GAS2L1 (Fig. 5, B and C).

We next used bacterial expression to obtain purified CH (i.e., 1–196) and CH-GAR (i.e., 1–300) proteins (Fig. S3 A) and then tested their direct interaction with F-actin in a cosedimentation assay: the recombinant proteins were incubated with preassembled F-actin, and after sedimentation, the proteins associated with F-actin were probed. The CH-GAR protein showed minimal F-actin-binding activity, which was 55% lower than the activity of the CH protein (Fig. 5 D). Moreover, preincubation of the CH protein with the GAR protein inhibited the cosedimentation of the CH protein with F-actin (Fig. 5 D). Collectively, these results revealed that the GAR domain exerts an inhibitory effect on the CH domain in GAS2L1. In these assays and in the microtubule sedimentation assays described below, the GAS2L1 proteins were not sedimented under control conditions in which the proteins were incubated in the absence of F-actin and microtubules (Fig. S3 B).

Similarly, we found that within GAS2L1, the CH domain inhibits the microtubule-binding activity of the GAR domain. We again used a cosedimentation assay to compare the microtubule-binding activity of GAR (i.e., 197–300) and CH-GAR proteins, and we found that this activity of the CH-GAR construct was 47%

lower than that of the GAR protein (Fig. 5 E). Furthermore, incubation of excess CH protein with GAR protein markedly reduced (by 43%) the cosedimentation of the GAR protein with microtubules (Fig. 5 E).

Considering the aforementioned results, we hypothesized that the CH and GAR domains physically interact with each other to exert the autoinhibitory effects. To test this, we coexpressed the CH and GAR constructs in cells, and we found robust coimmunoprecipitation of the GAR protein with the CH protein (Fig. 5 F). We also tested a GAS2L1 truncation construct lacking the CH and GAR domains (Tail; 300–681); this construct did not coimmunoprecipitate with the CH protein (Fig. 5 F). Therefore, the GAR domain is a unique GAS2L1 region that displays the CH-binding activity. The direct interaction between these two domains was validated in a binding assay performed using purified CH and GAR proteins; in this assay, CH protein pull-down with the GAR protein was readily detected (Fig. 5 G).

Ser352 phosphorylation relieves CH-GAR autoinhibition

To examine whether Ser352 phosphorylation interferes with the CH-GAR interaction and thereby relieves the autoinhibition, we engineered the S352A and S352D mutations into the CH-deleted construct (GAR-Tail; 197–681) and compared the CH-binding activity of the mutants in coimmunoprecipitation assays. Whereas the S352A mutant robustly coimmunoprecipitated with the CH protein, the S352D mutant showed substantially reduced CH-binding activity (Fig. 6 A). These results indicate that Ser352 phosphorylation disrupts the association between the CH and GAR domains.

We next tested the actin-binding activity of the WT and mutant proteins. GAS2L1 constructs were transiently expressed for pull-downs through the ectopic tag, and the captured proteins were immunoblotted for actin. Actin was specifically pulled down with all GAS2L1 proteins but at distinct levels: S352A and S352D showed ~62% lower and ~46% higher actin-binding activity, respectively, relative to WT GAS2L1 (Fig. 6 B). In a parallel experiment, transfected cells were treated with the F-actin-depolymerizing agent latrunculin B, and then cell extracts were prepared for the pull-down assay; the results showed that F-actin depolymerization abolished actin binding to the GAS2L1 proteins (Fig. 6 B). Together, the pull-down results indicate that GAS2L1 binds to F-actin but not G-actin, and further that GAS2L1 Ser352 phosphorylation drastically increases the F-actin-binding activity.

To assess the role of GAS2L1 phosphorylation at Ser352 in the centrosomal attachment of actin filaments, we determined the level of centrosome-associated F-actin in *gas2l1*^{-/-} cells stably expressing the GAS2L1 mutants S352A and S352D or the WT protein. Here, centrosome-associated F-actin was stained according to a published protocol (Farina et al., 2016), and for quantifying the F-actin, G2-phase cells were identified based on

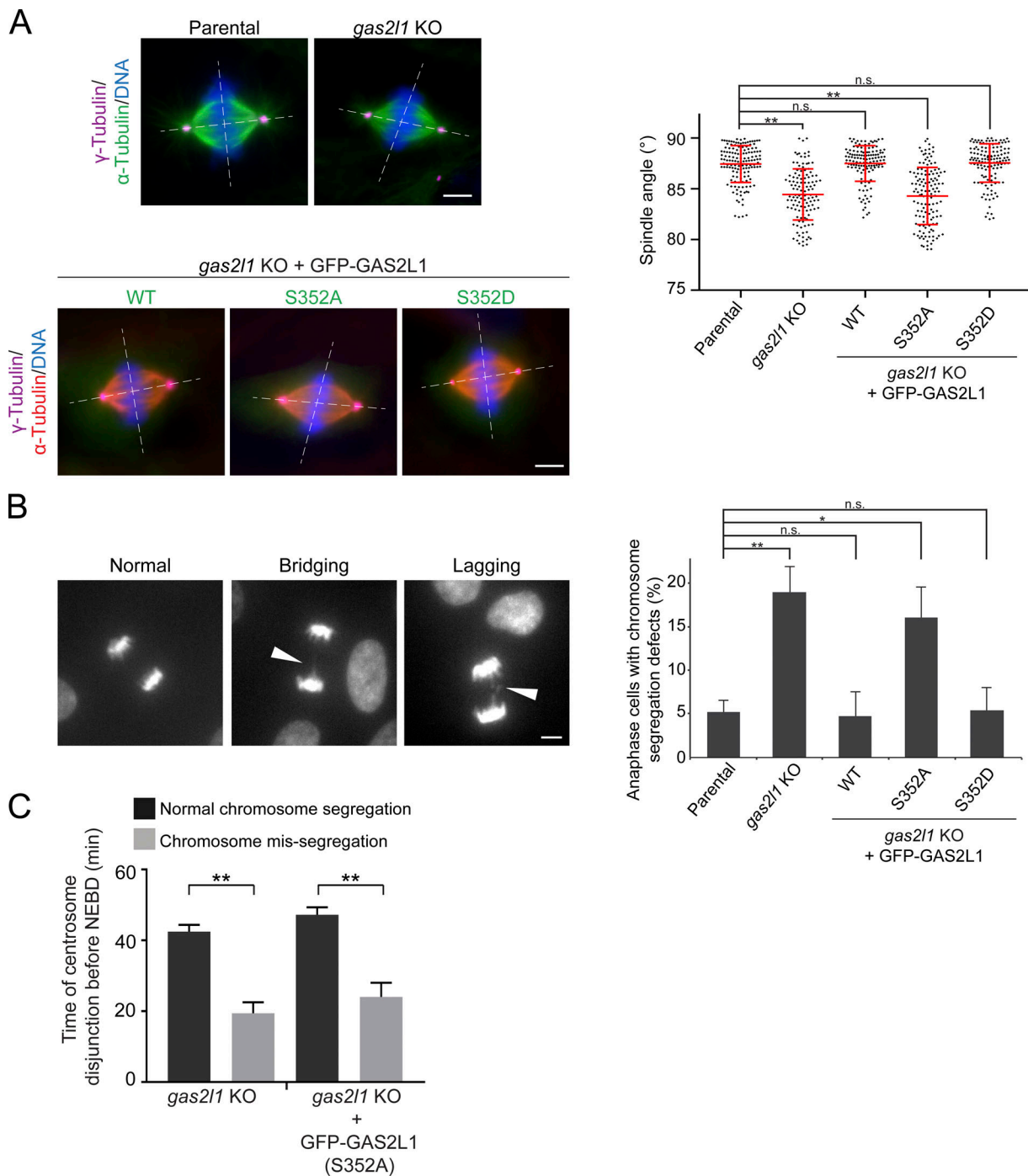


Figure 4. **GAS2L1 and its Ser352 phosphorylation are required for proper spindle organization and chromosome segregation.** (A) RPE-1 parental cells and sublines were stained for microtubules (anti- α -tubulin) and centrosomes (anti- γ -tubulin). The sublines examined were *gas2l1*-knockout line (*gas2l1* KO) and the knockout line stably expressing GFP-GAS2L1 (WT) or mutants (S352A and S352D). Angles between the spindle pole axis and the metaphase plate axis were determined from three repeats and are presented in a dot plot: $n = 143$ (parental), 123 (*gas2l1* KO), 131 (WT), 135 (S352A), and 136 (S352D). Midline: mean; upper and low lines: SD. One-way ANOVA; **, $P < 0.001$; n.s., not significant. (B) Time-lapse imaging of RPE-1 parental cells and sublines after incubation with 0.1 μ g/ml Hoechst 33342. Incidence of chromosome-segregation defects (bridging and lagging chromosomes) was quantified from three independent experiments: $n = 113$ (parental), 151 (*gas2l1* KO), 125 (WT), 118 (S352A), and 124 (S352D). Data are presented as means \pm SD of three experimental repeats. χ^2 test; *, $P < 0.01$; **, $P < 0.001$; n.s., not significant. Scale bars, 5 μ m. (C) Times of centrosome disjunction occurrence were determined from cells exhibiting normal segregation or mis-segregation of chromosomes. Data are presented as means \pm SEM. One-way ANOVA; **, $P < 0.001$.

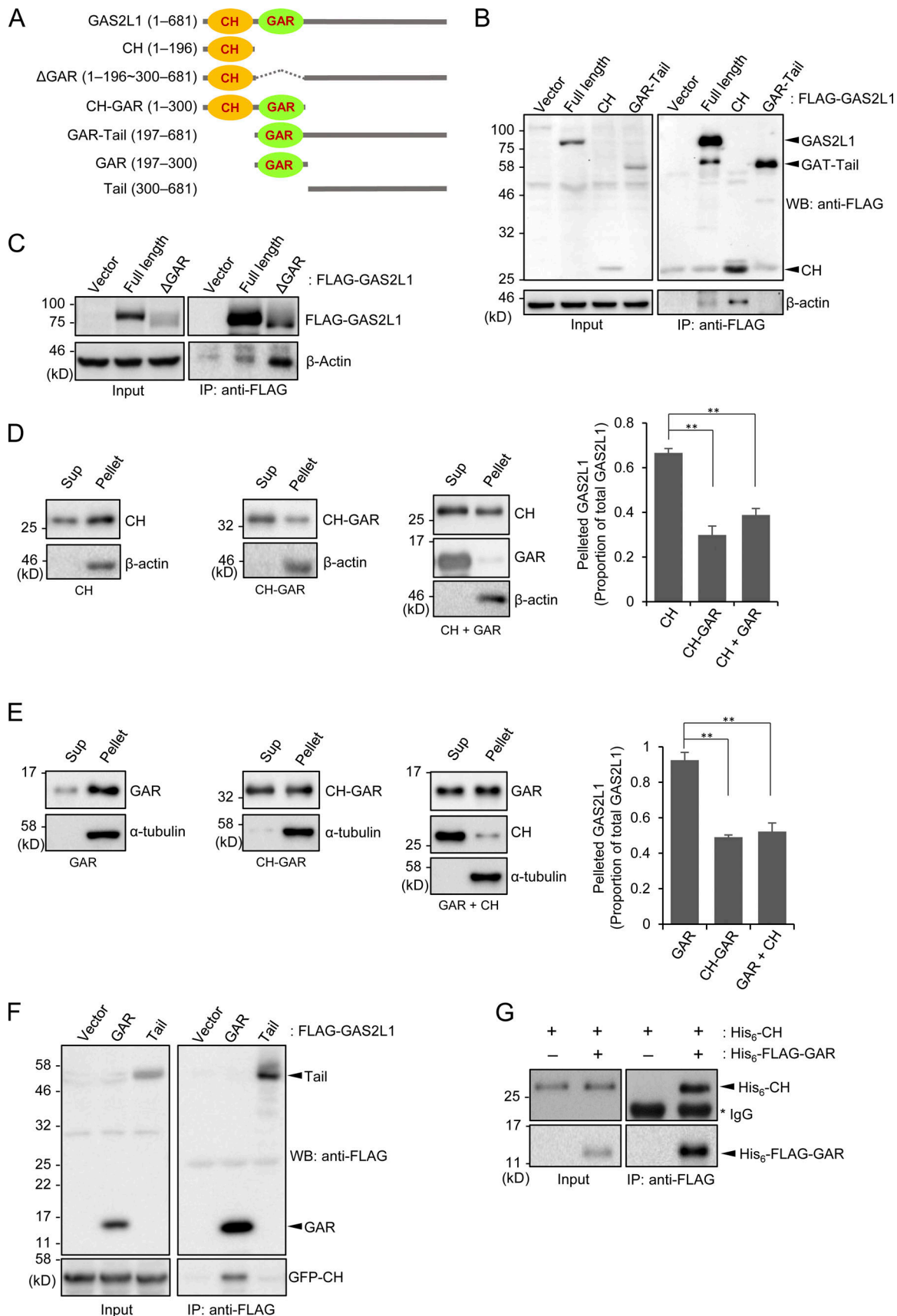


Figure 5. **GAS2L1 CH and GAR domains form an autoinhibitory module.** (A) Schematic of GAS2L1 fragments prepared for binding and sedimentation assays. (B and C) GAS2L1 constructs (FLAG-tagged) were transiently expressed in HEK293T cells for anti-FLAG immunoprecipitation. Samples of

immunoprecipitates (50%) and cell-lysate inputs (1%) were immunoblotted (WB) with antibodies against FLAG and β -actin. IP, immunoprecipitation; WB, Western blotting. **(D)** Recombinant GAS2L1 proteins (5 μ M; His₆-FLAG tagged) were incubated with polymerized F-actin. After sedimentation of F-actin, pellets and supernatants were collected for anti-His₆-tag and anti- β -actin immunoblotting. Sup, supernatant. To test the inhibitory effect of GAR protein, His₆-FLAG-CH (5 μ M) was preincubated with His₆-FLAG-GAR (25 μ M) for 30 min before binding with F-actin. Proportions of GAS2L1 proteins in pellets were quantified and are presented as means \pm SD of three independent assays. One-way ANOVA; **, $P < 0.001$. **(E)** His₆-FLAG-tagged GAS2L1 proteins (10 μ M) were incubated with taxol-stabilized microtubules in the sedimentation assay, and the distribution of the proteins into the microtubule pellets and the supernatants was probed by means of anti-His₆-tag and anti- α -tubulin immunoblotting. To test the effect of CH protein, His₆-FLAG-CH (50 μ M) was preincubated with His₆-FLAG-GAR (10 μ M) for 30 min. GAS2L1 proteins that cosedimented with microtubules were quantified, and the data are presented as means \pm SD of three independent experiments. One-way ANOVA; **, $P < 0.001$. **(F)** GAS2L1 fragments (FLAG-tagged) were transiently coexpressed in HEK293T cells with the CH domain (GFP-tagged) for anti-FLAG immunoprecipitation. Aliquots of immunoprecipitates (50%) and cell-lysate inputs (1%) were immunoblotted (WB) with antibodies against FLAG and GFP. **(G)** Recombinant proteins of CH domain (His₆ tagged; 2 μ M) and GAR domain (His₆-FLAG tagged; 1 μ M) were incubated, and the mixtures were then subject to anti-FLAG immunoprecipitation. Immunoprecipitates (50%) and inputs (5%) were analyzed through anti-His₆ immunoblotting.

cyclin B1 staining. Relative to cells expressing WT GAS2L1, S352A-expressing cells displayed a significantly reduced intensity (by \sim 31%) of centrosome-associated F-actin, but this intensity was not markedly altered relative to control in S352D-expressing cells (Fig. 6 C).

We sought to determine whether the amount of centrosome-associated actin changes when the cell cycle progresses to approach mitosis; thus, we quantified the actin level in G2 and non-G2 interphase cells, which show positive and negative staining for cyclin B1, respectively. The centrosome-associated F-actin appeared as a more robust meshwork in the G2 cells, and the F-actin intensity was \sim 34% higher than that in the non-G2 cells (Fig. 6 D). Therefore, the level of centrosome-associated F-actin is increased as a cell enters G2 and approaches mitosis.

To function in centrosome separation, GAS2L1 must localize at centrosomes and bind to F-actin, microtubules, and end-binding proteins such as EB1 (Au et al., 2017). To ascertain whether Ser352 phosphorylation affects GAS2L1 centrosomal localization, we visualized WT GAS2L1 and the mutants S352A and S352D in *gas2l1*^{-/-} cells stably expressing the proteins. The two mutants and the WT protein were detected at similar intensities at centrosomes (Fig. 2 C). We conclude that Ser352 phosphorylation does not alter the centrosomal localization of GAS2L1. We also tested WT GAS2L1 and the mutants S352A and S352D for EB1 interaction: in pull-down assays, the mutants and the WT protein showed similar EB1-binding activity (Fig. S4). These results suggest that Ser352 phosphorylation does not alter GAS2L1 interaction with EB1.

Nek2 mediates Ser352 phosphorylation in G2/M

After elucidating the function of GAS2L1 Ser352 phosphorylation, we searched for kinases that phosphorylate GAS2L1 at Ser352. Our immediate focus was on Nek2A because the kinase functions in late G2 to trigger centrosome disjunction. Moreover, RNAi-mediated silencing of Nek2 expression or the expression of kinase-dead Nek2A inhibits centrosome separation in G2/M (Faragher and Fry, 2003; Mardin et al., 2010). To test whether Nek2A phosphorylates GAS2L1 at Ser352, we examined the potential interaction between Nek2A and GAS2L1 by coexpressing GAS2L1 and a kinase-dead Nek2A mutant, Nek2A(K37R); because kinase-substrate interactions frequently are transient, we suspected that the interaction might be stabilized when the kinase-dead mutant is used. Accordingly, Nek2A(K37R) was readily detected in pull-downs of expressed GAS2L1, but it was not

detectable in pull-downs from vector-control cells (Fig. 7 A); these results revealed that Nek2A interacts specifically with GAS2L1.

When GAS2L1 was coexpressed with Nek2A, GAS2L1 was detected as a doublet in immunoblots (Fig. 7 B). Notably, the upper band disappeared when GAS2L1 was coexpressed with the kinase-dead mutant, Nek2A(K37R), or when extracts of cells coexpressing GAS2L1 and WT Nek2A were treated with alkaline phosphatase before SDS-PAGE (Fig. 7 B). Therefore, intact Nek2A caused the phosphorylation-dependent upshift of GAS2L1 from the transfected cells. Next, we ectopically expressed GAS2L1 and its S352A mutant and purified the proteins under a dephosphorylation condition. The purified samples contained primarily the intact proteins and a fragment of GAS2L1 (Fig. S5); the fragment was presumably a degradation product. When the proteins were used in an in vitro phosphorylation reaction with recombinant Nek2A, an SDS-PAGE mobility upshift of GAS2L1 was detected, and the upshift was eliminated by alkaline phosphatase treatment (Fig. 7 C); this is similar to what was observed in cells cotransfected with GAS2L1 and Nek2A (Fig. 7 B). Furthermore, the results of mass-spectrometric analysis identified Ser352 as one of the sites phosphorylated in vitro by Nek2A.

We also generated an antibody that specifically recognizes Ser352-phosphorylated GAS2L1, and we used the antibody for immunoblotting GAS2L1 phosphorylated in vitro by Nek2A. The anti-pSer352 antibody detected a doublet of phosphorylated GAS2L1, and it also detected a weak lower band of GAS2L1 not treated with Nek2A (Fig. 7 C). By contrast, the anti-pSer352 antibody did not detect any signal of the S352A mutant phosphorylated under the same conditions (Fig. 7 C). Together, these results confirmed the phosphorylation of GAS2L1 at Ser352 by Nek2 as well as the specificity of the anti-pSer352 antibody.

We next evaluated Ser352 phosphorylation in RPE-1 cells at various time points post-release from G1/S block. GAS2L1 appeared as a doublet at 12 h post-release, and Ser352 phosphorylation was strongly detected in the upper band of the doublet (Fig. 1 A and Fig. 7 D). By contrast, the phosphorylation was detected weakly at time points before 12 h post-release (Fig. 7 D). Therefore, Ser352 phosphorylation is drastically elevated in late G2 and mitosis, which correlates with the increased level of Nek2 on centrosomes (Fry et al., 1995, 1998b; Mardin et al., 2010). Moreover, RNAi-mediated depletion of Nek2 substantially reduced the level of Ser352 phosphorylation in cells synchronized to late G2 or M phase (Fig. 7 E), indicating that Nek2 is required for the phosphorylation.

indicated time points and analyzed by immunoblotting. **(E)** RPE-1 cells transfected with control siRNA (si-Control) or *nek2*-targeting siRNA (si-Nek2) were arrested with aphidicolin and then released into STLC-containing medium for 12 h. Cell extracts were immunoblotted with indicated antibodies. Intensity of Ser352-phosphorylated GAS2L1 was measured in GAS2L1 doublets and normalized and is presented as means \pm SD from three independent experiments. Unpaired Student's *t* test; **, $P < 0.001$. **(F)** HEK293T cells were transfected with GAS2L1 constructs and Nek2A WT or kinase-dead mutant K37R. After anti-FLAG immunoprecipitation, immunoprecipitates (50%) and lysate inputs (1%) were immunoblotted with anti-FLAG and anti-GFP antibodies. Anti-pSer352-GAS2L1 immunoblotting was also performed on lysate inputs. IP, immunoprecipitation. The coimmunoprecipitated CH domain was quantified and normalized and is presented as means \pm SD from three independent experiments. Unpaired Student's *t* test; ***, $P < 0.0001$. **(G)** GFP-GAS2L1 or the S352D mutant was overexpressed in asynchronous RPE-1 cells transfected with si-Control or si-Nek2. Centrosomes were labeled through anti- γ -tubulin staining. Boxed areas are enlarged; arrowheads: centrosomes. Centrosome distance was measured in GFP-GAS2L1- and S352D-expressing cells from three independent experiments: $n = 157$ (si-Control + GFP-GAS2L1 WT), 148 (si-Nek2 + GFP-GAS2L1 WT), 144 (si-Control + GFP-GAS2L1 S352D), and 161 (si-Nek2 + GFP-GAS2L1 S352D). χ^2 test; **, $P < 0.001$; n.s., not significant. Scale bars, 10 μ m in cell micrographs and 5 μ m in enlarged centrosome images.

the K37R-expressing cells, but this coimmunoprecipitation was almost undetectable from cells expressing WT Nek2A (Fig. 7 F). These results, together with those from the binding assays of the Ser352 mutants (Fig. 6 A), demonstrated that Ser352 phosphorylation by Nek2 disrupts the association of the CH and GAR domains.

We proceeded to examine whether Nek2 is required for the GAS2L1 function in centrosome disjunction. In agreement with our previous report (Au et al., 2017), GAS2L1 overexpression induced centrosome separation (Fig. 7 G). Nek2 knockdown blocked this effect of WT GAS2L1 overexpression but did not affect centrosome separation induced by the overexpression of the S352D mutant (Fig. 7 G). Therefore, Nek2 regulates the centrosome-separating function of GAS2L1 through Ser352 phosphorylation.

In late G2, Nek2 catalyzes the phosphorylation of several centrosome-linker components, such as rootletin and C-Nap1, which resolves the centrosome linker (Mardin and Schiebel, 2012). We sought to dissect the requirement of the two Nek2-mediated events—GAS2L1 phosphorylation and centrosome-linker disassembly—for centrosome disjunction. As previously reported (Fry et al., 1998a; Faragher and Fry, 2003), Nek2A overexpression resulted in centrosome separation in parental RPE-1 cells (Fig. 8 A). However, this effect of Nek2A overexpression was not observed in *gas2l1*^{-/-} cells (Fig. 8 A). These data indicate that GAS2L1 is indispensable for Nek2-mediated disjunction. We next evaluated the effect of Nek2-mediated GAS2L1 phosphorylation by using *gas2l1*^{-/-} cells stably expressing WT GAS2L1 or the S352D mutant. Expression of S352D at a level close to that of endogenous GAS2L1 did not trigger centrosome separation in non-G2 interphase cells (Fig. 2, B and C). Moreover, RNAi-mediated depletion of Nek2 blocked the centrosome separation occurring at G2 both in WT GAS2L1-expressing cells and S352D-expressing cells (Fig. 8 B). Similar effects of Nek2 knockdown were observed in Eg5-inhibited cells expressing either WT GAS2L1 or S352D, which were arrested in mitosis (Fig. 8 C). These results revealed that in the presence of the centrosome linker, GAS2L1 phosphorylation at Ser352 does not trigger centrosome disjunction.

To remove the centrosome linker, we used RNAi to silence rootletin expression (Bahe et al., 2005). Double-knockdown of Nek2 and rootletin inhibited centrosome separation in *gas2l1*^{-/-} cells stably expressing WT GAS2L1, but this inhibitory effect was not detected in knockout cells expressing the S352D mutant (Fig. 8, B and C). These results indicate that both GAS2L1

phosphorylation and centrosome-linker disassembly are necessary for centrosome disjunction, and further that the GAS2L1 phosphorylation and the linker disassembly act together to drive the disjunction.

Discussion

GAS2L1 is an organizer of actin filaments and microtubules at the proximal end of mature centrioles, and GAS2L1-mediated cytoskeletal attachments are indispensable for the dynamic movement of centrioles and the disjunction of duplicated centrosomes (Au et al., 2017). Here, we have identified a mechanism for the tight control of GAS2L1 functions, and we have revealed how GAS2L1 is activated for centrosome disjunction. Our key findings are the following: first, within GAS2L1, the functions of the CH and GAR domains are controlled by autoinhibition. Second, GAS2L1 displays G2/M-induced phosphorylation at several residues, one of which is Ser352; phosphorylation of Ser352 relieves the autoinhibition of the CH and GAR domains and thus is required for GAS2L1 functions in centrosome disjunction, spindle assembly, and chromosome segregation. Third, GAS2L1 Ser352 is phosphorylated in late G2 by Nek2, a kinase that also mediates centrosome-linker dissolution; notably, centrosome disjunction is induced when GAS2L1 phosphorylation occurs in conjunction with centrosome-linker disassembly.

In GAS2 family members, the CH domain is located near the amino terminus, and the CH domain is followed by the GAR domain and then an unstructured region of variable length (Stroud et al., 2014). The CH domain is present in proteins that perform diverse functions, and GAS2 and GAS2-like proteins contain a single type-3 CH domain (Gimona et al., 2002). We have provided evidence indicating that within GAS2L1, the CH and GAR domains bind directly to each other, and the interaction produces inhibitory effects on both domains. The CH-GAR autoinhibition is likely a feature of the GAS2 family. This notion is supported by the observation that in GAS2L3, deletion of the GAR domain augmented CH-domain binding to actin in transfected cells (Stroud et al., 2011). Both CH and GAR domains have also been found in spectraplakins (Suozzi et al., 2012), which are giant cytoskeletal cross-linkers. Spectraplakins harbor type-1/2 CH domains, which frequently exist in tandem, and the domains are located distant from the GAR domain in these proteins (Suozzi et al., 2012). Although this structural organization is distinct from that of GAS2-like proteins, interaction between the tandem CH domains near the amino terminus and the EF-hand-GAR near

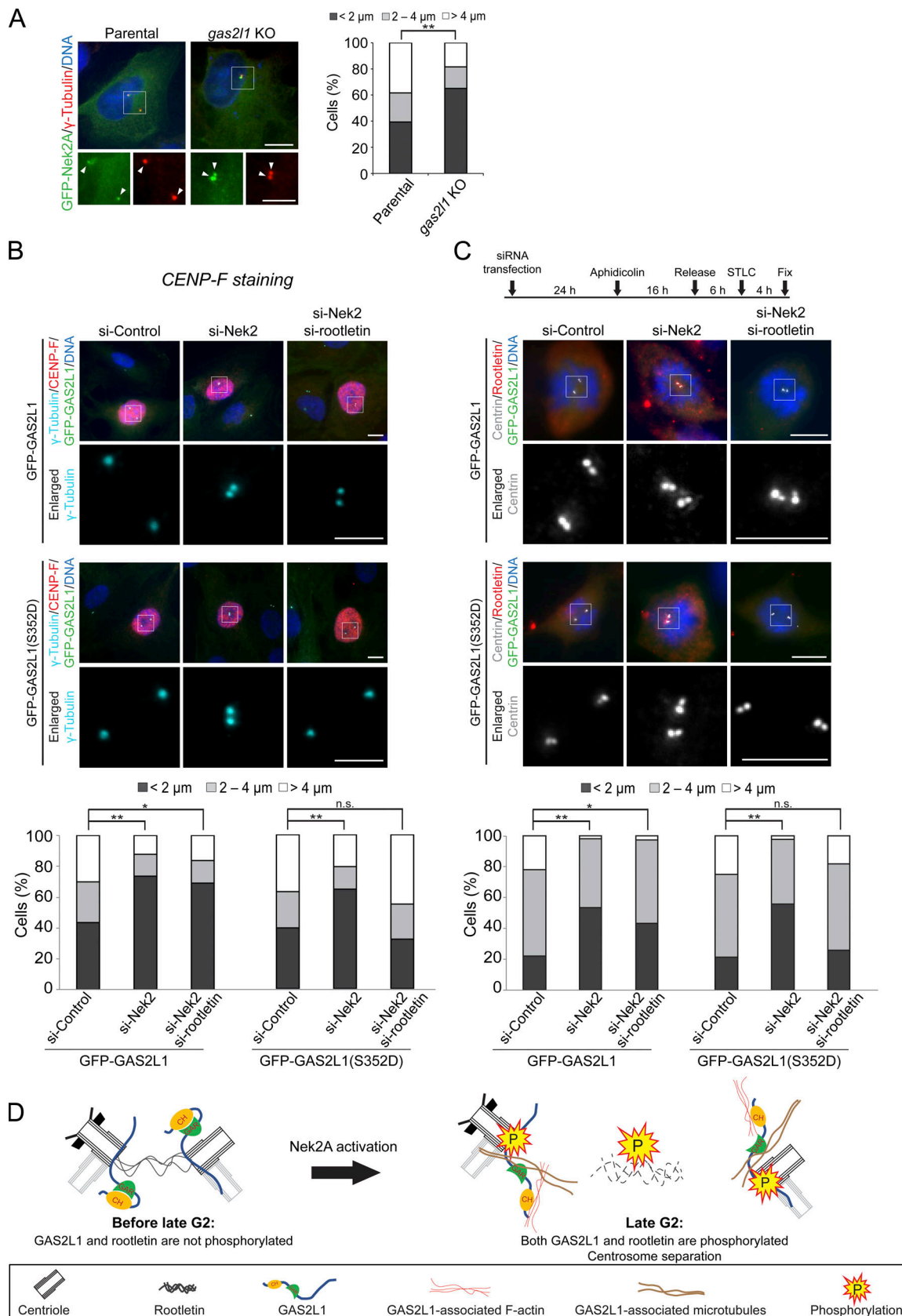


Figure 8. **Centrosome disjunction is mediated by GAS2L1 phosphorylation and centrosome-linker disassembly.** (A) RPE-1 parental cells and *gas2l1*-knockout line (GAS2L1 KO) were transfected with GFP-Nek2A and stained with anti- γ -tubulin. Boxed areas are enlarged; arrowheads: centrosomes. Centrosome distance was measured in asynchronous cells transfected with GFP-Nek2A from three independent experiments: $n = 112$ (parental) and 109 (GAS2L1

KO). Scale bars, 10 μm in cell micrographs and 5 μm in enlarged centrosome images. **(B)** RPE-1 *gas2l1*^{-/-} cells stably expressing GFP-GAS2L1 or the S352D mutant were transfected with indicated siRNAs. Centrosomes were labeled through anti- γ -tubulin staining; G2 cells were identified based on positive CENP-F staining. Centrosome distance was measured in G2 cells (CENP-F-positive cells) from three independent experiments: $n = 198$ (si-Control), 210 (si-Nek2), and 204 (si-Nek2 + si-rootletin). Boxed areas are enlarged. Scale bars, 10 μm in cell micrographs and 5 μm in enlarged centrosome images. **(C)** RPE-1 cells used as in B were synchronized with aphidicolin, released for 6 h, and treated with STLC for 4 h. Cells were stained for centrin and rootletin. Centrosome distance was measured in mitotic cells (arrested in prometaphase by STLC) from three independent experiments: GFP-GAS2L1 (WT) stable cells: $n = 125$ (si-Control), 136 (si-Nek2), and 119 (si-Nek2 + si-rootletin); GFP-GAS2L1 (S352D) stable cells: $n = 127$ (si-Control), 135 (si-Nek2), and 123 (si-Nek2 + si-rootletin). Arrowheads: centrosomes. Scale bars, 5 μm in cell micrographs and 2.5 μm in enlarged centrosome images. **(D)** Model depicting molecular events underlying centrosome disjunction. The disjunction is driven by GAS2L1 phosphorylation at Ser352 plus centrosome-linker disassembly, both of which are mediated by Nek2A. **(A–C)** χ^2 test; *, $P < 0.01$; **, $P < 0.001$; n.s., not significant.

the carboxy terminus has been detected in *Drosophila* Shot, a member of the spectraplakins family (Applewhite et al., 2013). Thus, spectraplakins likely retain the autoinhibition of the CH and GAR domains.

Here, we did not observe marked changes in GAS2L1 expression during the cell cycle, which agrees with a previous report (Wolter et al., 2012). However, GAS2L1 is hyperphosphorylated in late G2, and mitosis and the phosphorylation occur at several residues; these residues are all located within the unstructured tail region with the exception of Thr193 (Fig. 1), which is situated in the flexible region between the CH and GAR domains. Our mutational analyses revealed that the phosphorylation of one of these sites, Ser352, is required for centrosome disjunction, whereas the phosphorylation of the other residues is dispensable (Fig. 2 A and Fig. S1). Furthermore, the phosphorylation at Ser352 disrupted the association between the CH and GAR domains, which stimulated their F-actin- and microtubule-binding activities, respectively (Fig. 5 and Fig. 6); however, further investigation is necessary to determine how Ser352 phosphorylation disrupts this interaction.

GAS2L1 Ser352 phosphorylation occurs in a cell cycle-dependent manner: the phosphorylation was detected at low levels in interphase earlier than late G2 and was drastically elevated in late G2 and mitosis (Fig. 7 E). This strongly suggests that the actin- and microtubule-binding activities of GAS2L1 are maintained at low levels in interphase and then are markedly enhanced when cells approach mitosis. GAS2L1 functions in the motility of interphase centrosomes (Au et al., 2017), which requires the controlled binding of GAS2L1 to the cytoskeletons. GAS2-like proteins show little sequence homology in the tail region, except for the presence of an SxIP motif, and sequence alignment did not reveal any region in other GAS2-like proteins that is equivalent to Ser352 and its surrounding sequence in GAS2L1. This raises the possibility that the regulation of the CH and GAR domains by Ser352 phosphorylation is a unique property of GAS2L1.

Centrosome disjunction in late G2 is considered to require Nek2, which mediates centrosome-linker disassembly by phosphorylating several linker proteins, including C-Nap1, rootletin, Cep68, and LRRC45 (Fry et al., 1998a; Bahe et al., 2005; Graser et al., 2007; He et al., 2013). The disjunction also requires GAS2L1-mediated attachment of microtubules and F-actin to centrioles (Au et al., 2017); these cytoskeletons are considered to exert forces for driving centrosomes apart. Here, we have shown that Nek2A phosphorylates GAS2L1 at Ser352 to relieve GAS2L1 autoinhibition, and further that this GAS2L1 phosphorylation

and centrosome-linker disassembly occur concurrently and act together to split centrosomes, with neither step alone being sufficient for triggering centrosome disjunction (Fig. 8, A–C). Therefore, our findings reflect the concerted Nek2 actions that drive centrosomes apart (Fig. 8 D).

In the absence of Nek2-mediated disjunction, centrosomes can still be separated through the Eg5-driven mitotic pathway to assemble bipolar spindles, but the mitosis then tends to feature errors such as spindle-geometry defects, kinetochore mis-attachment, and chromosome mis-segregation (Kaseda et al., 2012; Silkworth et al., 2012; Zhang et al., 2012). Notably, cells harboring unseparated centrosomes at the NEBD stage show increased incidence of chromosome segregation errors (Kaseda et al., 2012; Silkworth et al., 2012). Presumably, Nek2-mediated centrosome disjunction facilitates the positioning of chromosomes in between the two separated centrosomes during prometaphase, which exposes the kinetochores to a high density of microtubules and thereby promotes the formation of amphitelic attachments (Magidson et al., 2011). We observed defects in spindle geometry and chromosome segregation in *gas2l1* knockout cells and in the cells rescued with the S352A mutant of GAS2L1 (Fig. 4), and these mitotic phenotypes are similar to those produced when Nek2 functions are disrupted (Faragher and Fry, 2003). Therefore, two Nek2-mediated events—removal of GAS2L1 autoinhibition and disassembly of the centrosome linker—together control the timely centrosome disjunction that is essential for error-free mitosis.

Materials and methods

Plasmids and siRNAs

Cloning and expression of human *gas2l1* were described previously (Au et al., 2017), and GAS2L1 mutants were generated using a PCR-based method of site-directed mutagenesis. The biotinylation (Bio)-2 \times TEV-EGFP-C1 vector and the BirA plasmid are described elsewhere (Jiang et al., 2014). To construct Bio-2 \times TEV-FLAG-C1, the EGFP sequence in the vector was replaced with the coding sequence of FLAG. GAS2L1 was subcloned into the biotinylation vectors by using standard molecular cloning techniques. For inducible expression, the coding sequence of GFP-GAS2L1 or its mutants was cloned together with a Kozak sequence into pRetroX-tight-pur (Clontech) by using the Gibson Assembly method (Gibson Assembly Master Mix, New England Biolabs). The constructs of GFP-Nek2A and its K37R mutant (Lou et al., 2004) were kindly provided by X. Yao (University of Science and Technology of China, Hefei, China). The following

siRNA oligonucleotides were purchased from GenePharma: *rootletin*, 5'-AAGCCAGUCUAGACAAGGATT-3' (Bahe et al., 2005); *nek2*, 5'-AAACAUCGUUCGUUACUUAU-3' (He et al., 2013); and negative-control siRNA, 5'-UUCUCGGAACGUGUCACGUTT-3'.

Antibodies

To generate a GAS2L1 phospho-Ser352-specific antibody, rabbits were immunized with the synthetic peptide HPRSRRYpSGDSDS-SAC (aa 345–359 of GAS2L1; Bio-Synthesis Inc.) conjugated to keyhole limpet hemocyanin (Imject Maleimide-Activated mckLH, Thermo Fisher Scientific). The obtained antisera were depleted for antibodies recognizing nonphosphorylated GAS2L1 by passing through a SulfoLink gel column (Thermo Fisher Scientific) coupled with the nonphosphorylated peptide (HPRSRRYSGDSDSSAC; Bio-Synthesis Inc.) before purification of phospho-specific antibodies by using the phosphorylated-peptide-coupled column. The phospho-specific antibodies were eluted from the column by using 100 mM glycine, pH 2.5, and dialyzed against PBS (137 mM NaCl, 2.7 mM KCl, 4.3 mM Na₂HPO₄, and 1.47 mM KH₂PO₄, pH 7.4) before storage. To generate an antibody against Nedd1, rabbits were immunized with His₆-Nedd1(321–660), and the resulting antisera were purified using immobilized GST-Nedd1(321–660). Antibodies against GAS2L1 and GFP were generated and used as described (Au et al., 2017). The following primary antibodies were from commercial sources: mouse anti- γ -tubulin (GTU-88; T5326, Sigma-Aldrich), goat anti- γ -tubulin (sc-7396, Santa Cruz), mouse anti- α -tubulin (DM1A; T6199, Sigma-Aldrich), mouse anti-Nek2 (610593, BD Biosciences), goat anti-rootletin (sc-67824, Santa Cruz), mouse anti-centrin (20H5; 04–1624, Millipore), mouse anti-FLAG (M2; F1804, Sigma-Aldrich), rabbit anti-FLAG (F7425, Sigma-Aldrich), mouse anti-GAPDH (6C5; AM4300, Thermo Fisher Scientific), mouse anti-cyclin B1 (GNS1; sc-245, Santa Cruz), mouse anti- β -actin (AC-74; A1978, Sigma-Aldrich), mouse anti-EB1 (610535, BD Biosciences), mouse anti-His₆ (sc-8036, Santa Cruz), and rabbit anti-pericentrin (ab4448, Abcam).

Cell cultures and treatments

All cell lines used in this study were obtained from American Type Culture Collection. HEK293T, HeLa, and Phoenix-AMPHO cells were maintained in DMEM (Gibco) supplemented with 10% FBS and 1% penicillin/streptomycin. RPE-1 cells were cultured in DMEM/Ham's F12 (1:1) containing 10% FBS, 1% penicillin/streptomycin, and 10 μ g/ml hygromycin B (Sigma-Aldrich). All cells were grown in a humidified environment containing 5% CO₂ at 37°C and were free of mycoplasma contamination. Plasmids were transfected into RPE-1 and HeLa cells by using FuGENE HD (Promega) and into HEK293T and Phoenix-AMPHO cells by using polyethylenimine (Polysciences); siRNAs were transfected using Lipofectamine 2000 or Lipofectamine RNAi-Max (Thermo Fisher Scientific).

To arrest the cell cycle at G1/S, RPE-1 cells were cultured in medium containing 1.6 μ g/ml aphidicolin (Sigma-Aldrich) for 18 h, and HeLa cells were cultured in medium containing 2 mM thymidine (Sigma-Aldrich) for 16 h. The cells were then released from the G1/S block into medium containing 5 μ M STLC (Sigma-Aldrich) and cultured for various times. RPE-1 cells were mitotically synchronized by releasing cells from the G1/S block for

6 h and then treating the cells with 100 nM nocodazole (Sigma-Aldrich) for 12 h. Mitotic cells were collected by shaking off rounded cells. To inhibit Eg5 and analyze Eg5-independent centrosome separation, RPE-1 cells released for 6 h from the G1/S block were treated for 4 h with 5 μ M STLC. Actin filaments were disrupted by treating cells with 1 μ M latrunculin B (Sigma-Aldrich) for 1 h.

Generation of GAS2L1-knockout and stable-expression cells

GAS2L1-knockout lines of RPE-1 cells were generated using the CRISPR/Cas9 system. A *gas2l1*-targeting sequence (5'-CACCGGGCA GCCTCGGTACAGGCGT-3') was engineered into pSpCas9(BB)-2A-Puro (PX459; 48139, Addgene; Ran et al., 2013) for transfection into RPE-1 cells. After transfection, the cells were selected with 20 μ g/ml puromycin (Sigma-Aldrich) for 4 d and then recovered in drug-free medium for approximately 1 wk. Single clones of the cells were isolated, and GAS2L1 knockout was confirmed by DNA sequencing and immunoblotting.

In rescue experiments, GFP-GAS2L1 was expressed in *gas2l1*^{-/-} RPE-1 cells by using a Tet-On expression system based on the retroviral pRetroX-based vectors pRetroX-tight-pur and pRetroX-Tet-On Advanced (Clontech). After viral packaging in Phoenix-AMPHO cells, the retrovirus-enriched media were collected, passed through a 0.45- μ m filter, and used for infection. To establish stable lines of GFP-GAS2L1, *gas2l1*^{-/-} RPE-1 cells were first infected with the pRetroX-Tet-On Advanced virus and selected with 800 μ g/ml G418 for ~2 wk, and then infected with the pRetroX-Tight-Pur-GFP-GAS2L1 virus and further selected with 10 μ g/ml puromycin and 400 μ g/ml G418 for ~2 wk. Individual clones were isolated and cultured. Without incubation with doxycycline, the leakage expression of GFP-GAS2L1 and its mutants in the clones was comparable with the level of GAS2L1 in parental RPE-1 cells.

Immunofluorescence microscopy

Cells grown on 18-mm coverslips were fixed with methanol for 5 min at -20°C and post-fixed with 4% paraformaldehyde in PBS, unless specifically described otherwise. The cells were then washed with PBS containing 0.05% Tween 20 and blocked with 2% bovine serum albumin in the same buffer. The cells were next sequentially stained (at room temperature) with primary antibodies and fluorophore-conjugated secondary antibodies (fluorophores: Alexa Fluor 488/568/594/647; Invitrogen). Nuclear DNA was labeled with 1 μ M Hoechst 33258 (Sigma-Aldrich). Fluorescence images were acquired using an Axio Observer ZI (Carl Zeiss) with a Plan Apo 100 \times NA 1.4 oil objective. The microscope was equipped with an X-Cite series 120Q lamp (Lumen Dynamics), a DAPI/GFP/Texas-Red/Cy5 optical filter unit (Carl Zeiss), and an sCMOS camera (Orca-Flash4.0, Hamamatsu); the acquired images were analyzed and processed using ZEN 2012 or ZEN 3.0 (blue edition) software (Carl Zeiss).

Intercentrosome distances were measured using the Line tool of ZEN software. Angles between the axis of the two spindle poles and the long axis of the metaphase plate were measured using the Angle tool in the Fiji package of ImageJ (Schindelin et al., 2012): the pole-to-pole spindle axis was the line that passed through the center of the two spindle poles; the long axis

of the metaphase plate was the midline of the long side of the plate. The acute angles were presented when they were not at a right angle. Centrosomal intensities of γ -tubulin and pericentrin were determined using the Circle tool of ZEN software: staining intensities were measured within a 2- μ m-diameter circle surrounding the centrosomes; moreover, background signal was acquired from a cytoplasmic area of the same size for subtraction.

In microtubule regrowth assays, cellular microtubules were depolymerized on ice water for 1 h, and then the regrowth was initiated at room temperature and allowed to proceed for 1 min (Choi et al., 2010; Shen et al., 2017). Following microtubule regrowth, the cells were fixed with 4% paraformaldehyde in PHEM buffer (60 mM Pipes, 25 mM Hepes, pH 6.9, 10 mM EGTA, and 2 mM $MgCl_2$) containing 2% sucrose and 0.2% Triton X-100 for immunostaining. The fluorescence intensity of microtubule asters was measured from a 4- μ m-diameter circle enclosing the asters, and background acquired from a cytoplasmic area of the same size was subtracted.

Centrosome-associated F-actin was quantified in non-G2 cells (cyclin B1-negative) and G2 cells (cyclin B1-positive) before centrosome separation ($d < 2 \mu$ m; measured using the Line tool of ZEN software). To visualize centrosome-associated F-actin, cells were detached by trypsinization, pelleted, and fixed with 4% paraformaldehyde in PBS. Next, the cells were incubated overnight at 4°C on poly-D-lysine-coated coverslips, permeabilized in 0.2% Triton X-100 for 2 min, and then sequentially stained with primary and secondary antibodies. F-actin was stained for 30 min with Alexa Fluor 350/647-phalloidin (Invitrogen). The fluorescence intensity of centrosome-associated F-actin was measured in a 3- μ m-diameter circle by using ZEN 2012 software. Background fluorescence was acquired from a cytoplasmic area of same size lacking F-actin and was subtracted from the intensities measured at centrosomes.

Time-lapse imaging

Time-lapse imaging was conducted to capture centrosome dynamics before NEBD and to monitor mitotic progression. Cells were seeded on 96-well optical polystyrene-bottom plates and imaged in the presence of 0.1 μ M SiR-tubulin and 10 μ M verapamil (Cytoskeleton Inc.) on a Cell Discoverer 7 automated microscope (Carl Zeiss) with a Plan Apo 50 \times NA 1.2 water objective. The microscope was equipped with an incubation system to maintain an environment of 37°C with 5% humidified CO_2 , LEDs for fluorescence excitation, and an Orca-Flash4.0 V3 Digital CMOS camera (Hamamatsu). Image sequences were captured at 8-min intervals, and Z stacks composed of five 3- μ m steps were acquired at each time point. The duplicated centrosomes remained in the same stack in all analyzed cells before mitotic entry, after which the separated centrosomes were observed in distinct stacks. Stacks containing centrosomes were subject to maximum-intensity projection by using ZEN 3.0 software (blue edition), and the image sequences were processed using the Fiji package of ImageJ. Intercentrosome distances were measured using the Line selection tool in the Fiji package of ImageJ, and $d > 2 \mu$ m was taken as centrosome separation.

To image chromosome segregation during anaphase, cells were grown on 25-mm coverslips. Before imaging, the cells were

incubated with 0.1 μ g/ml Hoechst 33342 (Sigma-Aldrich) for 30 min. Images of anaphase cells were captured using a Ti-E Nikon inverted microscope with a Plan Fluor 40 \times NA 0.6 dry objective. The microscope was equipped with an incubation chamber that maintained an atmosphere of 37°C and 5% humidified CO_2 (Chamlide), a Perfect Focus System, an epifluorescence illuminator (Nikon), a Lambda 10-3 filter wheel with a Uniblitz shutter (Sutter Instrument Co.), and a Zyla ultra-low-noise sCMOS camera (Andor Technology). Cell images were analyzed using the Fiji package of ImageJ.

Protein analysis by mass spectrometry

Cells ectopically expressing GAS2L1 were extracted with RIPA buffer (20 mM Tris-HCl, pH 7.4, 1% Triton X-100, 0.1% SDS, 0.5% sodium deoxycholate, 150 mM NaCl, 10 mM $MgCl_2$, 1 mM dithiothreitol, and Roche Complete Protease Inhibitor Cocktail), and the extracts were clarified by centrifugation (16,000 g , 15 min). The expressed GFP-GAS2L1 was immunoprecipitated through the ectopic tag, and the immunoprecipitates were resolved using SDS-PAGE and stained with Coomassie Blue. The GAS2L1 protein bands excised from SDS-PAGE gels were reduced with dithiothreitol, alkylated with iodoacetamide, and digested with trypsin. Following peptide extraction, the peptides were analyzed using mass spectrometry (LTQ Velos Dual-Pressure Ion Trap Mass Spectrometer, Thermo Fisher Scientific) coupled with reverse-phase liquid chromatography. The obtained tandem mass spectra were subject to searches in a gene database by using the MASCOT search engine (Matrix Science) for protein and phosphorylation site identification.

Recombinant protein preparation

Recombinant GAS2L1 proteins containing a His₆ or His₆-FLAG tag were expressed in *Escherichia coli* BL21 (DE3), purified using Ni²⁺-nitrilotriacetic acid resin (Qiagen), and dialyzed in PBS containing 10% glycerol. Proteins used in F-actin sedimentation assays were dialyzed in G-buffer (5 mM Tris-HCl, pH 8.0, and 0.2 mM $CaCl_2$). After dialysis, the proteins were stored in aliquots at -80°C.

F-actin sedimentation assay

Rabbit skeletal muscle G-actin (>99% purity; Cytoskeleton Inc.) was diluted in G-buffer containing 0.2 mM ATP and 0.5 mM dithiothreitol, and GAS2L1 proteins (His₆-FLAG tagged) were diluted in actin polymerization buffer (10 mM Tris-HCl, pH 7.5, 50 mM KCl, 2 mM $MgCl_2$, and 1 mM ATP); the G-actin and GAS2L1 proteins were then clarified by centrifugation at 150,000 g at 4°C for 30 min. Next, F-actin was polymerized in the actin polymerization buffer for 1 h at room temperature, and the F-actin polymerized from 5 μ M G-actin was incubated with the GAS2L1 proteins (5 μ M) in the polymerization buffer for 30 min at room temperature. Last, the samples were centrifuged at 150,000 g for 30 min at 24°C, and then both the supernatants and the pellets were analyzed on immunoblots.

Microtubule sedimentation assay

Purification of porcine brain microtubule-associated protein-free α/β -tubulin was described previously (Hou et al., 2007). Before assays, α/β -tubulin and GAS2L1 proteins (His₆-FLAG

tagged) were diluted in BRB80 buffer (80 mM K-Pipes, pH 6.9, 1 mM EGTA, and 1 mM MgCl₂) supplemented with 1 mM GTP and 1 mM dithiothreitol, and then clarified by centrifugation at 150,000 *g* for 30 min at 4°C. Microtubules were polymerized at 37°C with taxol (Selleckchem) at 0.2 μM for 5 min, 2 μM for 5 min, and then 20 μM for 15 min. After polymerization, microtubules assembled from 2 μM α/β-tubulin were incubated with the GAS2L1 proteins (10 μM) for 30 min at 30°C. Subsequently, the samples were overlaid on a glycerol cushion (40% glycerol in BRB80 buffer) and centrifuged at 100,000 *g* for 30 min at 30°C (Hou et al., 2007), and the obtained supernatant and pellet fractions were analyzed through immunoblotting.

Protein binding assays

HEK293T cells expressing FLAG-tagged GAS2L1 proteins were extracted in lysis buffer (50 mM Hepes, pH 7.4, 0.5% Triton X-100, 150 mM NaCl, 1 mM MgCl₂, 10 mM NaF, 1 mM dithiothreitol, and Roche Complete Protease Inhibitor Cocktail), and the extracts were clarified by centrifugation at 16,000 *g* for 15 min at 4°C. FLAG-tagged or His₆-FLAG-tagged GAS2L1 was immunoprecipitated with ANTI-FLAG M2 Affinity Agarose Gel (Sigma-Aldrich) at 4°C for 2 h with rotation, and the collected beads were washed extensively with lysis buffer and boiled at 95°C for use in SDS-PAGE and immunoblotting. To test the binding between the GAS2L1 proteins and actin filaments, cell extraction and anti-FLAG immunoprecipitation were performed in F-actin buffer (50 mM Pipes, pH 6.9, 0.5% Triton X-100, 50 mM NaCl, 5 mM MgCl₂, 5 mM EGTA, 5% glycerol, 1 mM ATP, 1 mM dithiothreitol, and Roche Complete Protease Inhibitor Cocktail), modified from previous reports (Algeciras-Schminich and Peter, 2003; Tang and Gunst, 2004; Legrand-Poels et al., 2007). In vitro binding assays were performed in a binding buffer (50 mM Hepes, pH 7.4, 0.1% Triton X-100, 150 mM NaCl, 1 mM MgCl₂, and 1 mM dithiothreitol) containing 1 mg/ml bovine serum albumin.

To perform pull-downs through the biotinylation tag, GAS2L1 tagged with Bio-2×TEV-FLAG or Bio-2×TEV-GFP was coexpressed with BirA in HEK293T cells cultured in DMEM/Ham's F10 medium (1:1 ratio) containing 10% FBS and 1% penicillin/streptomycin. Cells were extracted in lysis buffer, and the extracts were clarified by centrifugation at 16,000 *g* for 15 min at 4°C. Ectopically expressed GAS2L1 was pulled down using Dynabeads M-280 Streptavidin (Invitrogen) for 2 h at 4°C with rotation. To analyze GAS2L1-associated proteins, the beads were washed extensively with lysis buffer lacking dithiothreitol and the protease inhibitors, and then boiled for SDS-PAGE and immunoblotting.

In vitro phosphorylation

GFP-GAS2L1 was expressed in fusion with a biotinylation tag and was pulled down using streptavidin-coupled beads. After washing with phosphatase buffer (50 mM Hepes, pH 8.0, 0.1% Triton X-100, 100 mM NaCl, and 10 mM MgCl₂), the beads were treated with calf intestinal phosphatase (New England Biolabs) at 37°C for 1 h; subsequently, the beads were washed sequentially with lysis buffer containing 1 M NaCl and the cleavage buffer of tobacco etch virus (TEV) protease (50 mM Hepes, pH 7.4, 0.05% Triton X-100, 150 mM NaCl, 1 mM MgCl₂, 1 mM

EGTA, and 1 mM dithiothreitol). GFP-GAS2L1 was retrieved through cleavage with TEV protease. The purified GFP-GAS2L1 protein (0.5 μg) was phosphorylated at 30°C for 1 h with 50 ng of Nek2A kinase (GST-tagged; Abcam) in kinase buffer (50 mM Tris-HCl, pH 7.7, 10 mM MgCl₂, 1 mM dithiothreitol, 10 mM NaF, and 0.1 mM ATP). Reactions were terminated by adding SDS-PAGE sample buffer and boiling at 95°C. GAS2L1 phosphorylation was detected through anti-phospho-GAS2L1 (pSer352) immunoblotting.

Statistical analyses

All quantification datasets were collected from at least three independent experiments. Statistical analyses were performed using GraphPad Prism software, and the statistical tests used are indicated in the figure legends. *P* values were calculated using unpaired Student's *t* test for two given samples, one-way ANOVA test for differences across more than two sample groups, and χ² test for the difference in distributions across categories of inter-centrosome distances; *P* > 0.05 was considered statistically not significant. Data distribution was considered to be normal for parametric Student's *t* test and ANOVA test.

Online supplemental material

Fig. S1 (related to Fig. 2) shows that Ser-to-Ala substitution at position 355, 357, 358, or 360 does not affect the centrosome-separating activity of GAS2L1. Fig. S2 (related to Fig. 3 and Fig. 4) shows that *gas2li* knockout and GAS2L1 phosphorylation at Ser352 do not affect centrosome maturation. Fig. S3 (related to Fig. 5) shows the analysis of purified recombinant GAS2L1 fragments. Fig. S4 (related to Fig. 6) shows that the EB1 binding activity of GAS2L1 is unaffected by Ser352 phosphorylation. Fig. S5 (related to Fig. 7) shows the analysis of GAS2L1 proteins ectopically expressed in HEK293T cells and purified. Videos 1, 2, 3, 4, and 5 are the time-lapse imaging videos of parental, *gas2li*^{-/-} cells, and *gas2li*^{-/-} cells expressing WT, S352A, and S352D GAS2L1 as the cells progressed into mitosis.

Acknowledgments

We thank Dr. Anna Akhmanova for communication of unpublished data and critical reading of the manuscript, Dr. Xuebiao Yao (University of Science and Technology of China, Hefei, China) for providing GFP-Nek2A constructs, Dr. Feng Zhang (Broad Institute of Massachusetts Institute of Technology and Harvard University, Cambridge, MA) for the pSpCas9(BB)-2A-Puro plasmid, and Dr. Yusong Guo (The Hong Kong University of Science and Technology, Hong Kong, China) for sharing tools and reagents.

This work was supported by the General Research Fund (16100215, 16101717, and 16101418) and the Hong Kong Research Grants Council Theme-based Research Scheme (T13-605/18-W), Shenzhen Science and Technology Committee Research Grants (JCYJ20170818113915877, CKFW2016082916015476, and ZDSYS201707281432317), and the Innovation and Technology Commission – Hong Kong (ITCPD/17-9).

The authors declare no competing financial interests.

Author contributions: Conceptualization and methodology, F.K.C. Au and R.Z. Qi; investigation, F.K.C. Au and B.K.T. Hau; writing – original draft, F.K.C. Au and R.Z. Qi; writing – review

and editing, F.K.C. Au, B.K.T. Hau, and R.Z. Qi; supervision and funding acquisition, R.Z. Qi.

Submitted: 16 September 2019

Revised: 16 January 2020

Accepted: 28 February 2020

References

- Agircan, F.G., E. Schiebel, and B.R. Mardin. 2014. Separate to operate: control of centrosome positioning and separation. *Philos. Trans. R. Soc. Lond. B Biol. Sci.* 369:20130461. <https://doi.org/10.1098/rstb.2013.0461>
- Algeciras-Schimmich, A., and M.E. Peter. 2003. Actin dependent CD95 internalization is specific for Type I cells. *FEBS Lett.* 546:185–188. [https://doi.org/10.1016/S0014-5793\(03\)00558-1](https://doi.org/10.1016/S0014-5793(03)00558-1)
- Applewhite, D.A., K.D. Grode, M.C. Duncan, and S.L. Rogers. 2013. The actin-microtubule cross-linking activity of *Drosophila* Short stop is regulated by intramolecular inhibition. *Mol. Biol. Cell.* 24:2885–2893. <https://doi.org/10.1091/mbc.e12-11-0798>
- Au, F.K.C., Y. Jia, K. Jiang, I. Grigoriev, B.K.T. Hau, Y. Shen, S. Du, A. Akhmanova, and R.Z. Qi. 2017. GAS2L1 Is a Centriole-Associated Protein Required for Centrosome Dynamics and Disjunction. *Dev. Cell.* 40:81–94. <https://doi.org/10.1016/j.devcel.2016.11.019>
- Bahe, S., Y.-D. Stierhof, C.J. Wilkinson, F. Leiss, and E.A. Nigg. 2005. Rootletin forms centriole-associated filaments and functions in centrosome cohesion. *J. Cell Biol.* 171:27–33. <https://doi.org/10.1083/jcb.200504107>
- Blangy, A., H.A. Lane, P. d'Hérin, M. Harper, M. Kress, and E.A. Nigg. 1995. Phosphorylation by p34cdc2 regulates spindle association of human Eg5, a kinesin-related motor essential for bipolar spindle formation in vivo. *Cell.* 83:1159–1169. [https://doi.org/10.1016/0092-8674\(95\)90142-6](https://doi.org/10.1016/0092-8674(95)90142-6)
- Burakov, A., E. Nadezhkina, B. Slepchenko, and V. Rodionov. 2003. Centrosome positioning in interphase cells. *J. Cell Biol.* 162:963–969. <https://doi.org/10.1083/jcb.200305082>
- Cao, J., J. Crest, B. Fasulo, and W. Sullivan. 2010. Cortical actin dynamics facilitate early-stage centrosome separation. *Curr. Biol.* 20:770–776. <https://doi.org/10.1016/j.cub.2010.02.060>
- Choi, Y.-K., P. Liu, S.K. Sze, C. Dai, and R.Z. Qi. 2010. CDK5RAP2 stimulates microtubule nucleation by the γ -tubulin ring complex. *J. Cell Biol.* 191:1089–1095. <https://doi.org/10.1083/jcb.201007030>
- Fang, G., D. Zhang, H. Yin, L. Zheng, X. Bi, and L. Yuan. 2014. Centlein mediates an interaction between C-Nap1 and Cep68 to maintain centrosome cohesion. *J. Cell Sci.* 127:1631–1639. <https://doi.org/10.1242/jcs.139451>
- Faragher, A.J., and A.M. Fry. 2003. Nek2A kinase stimulates centrosome disjunction and is required for formation of bipolar mitotic spindles. *Mol. Biol. Cell.* 14:2876–2889. <https://doi.org/10.1091/mbc.e03-02-0108>
- Farina, F., J. Gaillard, C. Guérin, Y. Couté, J. Sillibourne, L. Blanchoin, and M. Théry. 2016. The centrosome is an actin-organizing centre. *Nat. Cell Biol.* 18:65–75. <https://doi.org/10.1038/ncb3285>
- Fletcher, L., G.J. Cerniglia, T.J. Yen, and R.J. Muschel. 2005. Live cell imaging reveals distinct roles in cell cycle regulation for Nek2A and Nek2B. *Biochim. Biophys. Acta.* 1744:89–92. <https://doi.org/10.1016/j.bbamer.2005.01.007>
- Fry, A.M., S.J. Schultz, J. Bartek, and E.A. Nigg. 1995. Substrate specificity and cell cycle regulation of the Nek2 protein kinase, a potential human homolog of the mitotic regulator NIMA of *Aspergillus nidulans*. *J. Biol. Chem.* 270:12899–12905. <https://doi.org/10.1074/jbc.270.21.12899>
- Fry, A.M., T. Mayor, P. Meraldi, Y.D. Stierhof, K. Tanaka, and E.A. Nigg. 1998a. C-Nap1, a novel centrosomal coiled-coil protein and candidate substrate of the cell cycle-regulated protein kinase Nek2. *J. Cell Biol.* 141:1563–1574. <https://doi.org/10.1083/jcb.141.7.1563>
- Fry, A.M., P. Meraldi, and E.A. Nigg. 1998b. A centrosomal function for the human Nek2 protein kinase, a member of the NIMA family of cell cycle regulators. *EMBO J.* 17:470–481. <https://doi.org/10.1093/emboj/17.2.470>
- Jimona, M., K. Djinovic-Carugo, W.J. Kranewitter, and S.J. Winder. 2002. Functional plasticity of CH domains. *FEBS Lett.* 513:98–106. [https://doi.org/10.1016/S0014-5793\(01\)03240-9](https://doi.org/10.1016/S0014-5793(01)03240-9)
- Goriounov, D., C.L. Leung, and R.K.H. Liem. 2003. Protein products of human Gas2-related genes on chromosomes 17 and 22 (hGAR17 and hGAR22) associate with both microfilaments and microtubules. *J. Cell Sci.* 116:1045–1058. <https://doi.org/10.1242/jcs.00272>
- Graser, S., Y.-D. Stierhof, and E.A. Nigg. 2007. Cep68 and Cep215 (Cdk5rap2) are required for centrosome cohesion. *J. Cell Sci.* 120:4321–4331. <https://doi.org/10.1242/jcs.020248>
- He, R., N. Huang, Y. Bao, H. Zhou, J. Teng, and J. Chen. 2013. LRRC45 is a centrosome linker component required for centrosome cohesion. *Cell Rep.* 4:1100–1107. <https://doi.org/10.1016/j.celrep.2013.08.005>
- Hou, Z., Q. Li, L. He, H.-Y. Lim, X. Fu, N.S. Cheung, D.X. Qi, and R.Z. Qi. 2007. Microtubule association of the neuronal p35 activator of Cdk5. *J. Biol. Chem.* 282:18666–18670. <https://doi.org/10.1074/jbc.C700052200>
- Jiang, K., G. Toedt, S. Montenegro Gouveia, N.E. Davey, S. Hua, B. van der Vaart, I. Grigoriev, J. Larsen, L.B. Pedersen, K. Bezstarosti, et al. 2012. A Proteome-wide screen for mammalian SxIP motif-containing microtubule plus-end tracking proteins. *Curr. Biol.* 22:1800–1807. <https://doi.org/10.1016/j.cub.2012.07.047>
- Jiang, K., S. Hua, R. Mohan, I. Grigoriev, K.W. Yau, Q. Liu, E.A. Katrukha, A.F.M. Altelaar, A.J.R. Heck, C.C. Hoogenraad, and A. Akhmanova. 2014. Microtubule minus-end stabilization by polymerization-driven CAM-SAP deposition. *Dev. Cell.* 28:295–309. <https://doi.org/10.1016/j.devcel.2014.01.001>
- Joukov, V., J.C. Walter, and A. De Nicolo. 2014. The Cep192-organized aurora A-Plk1 cascade is essential for centrosome cycle and bipolar spindle assembly. *Mol. Cell.* 55:578–591. <https://doi.org/10.1016/j.molcel.2014.06.016>
- Kaseda, K., A.D. McAnish, and R.A. Cross. 2012. Dual pathway spindle assembly increases both the speed and the fidelity of mitosis. *Biol. Open.* 1:12–18. <https://doi.org/10.1242/bio.2011012>
- Kimura, K., and A. Kimura. 2011. A novel mechanism of microtubule length-dependent force to pull centrosomes toward the cell center. *Bio-architecture.* 1:74–79. <https://doi.org/10.4161/bioa.1.2.15549>
- Lane, H.A., and E.A. Nigg. 1996. Antibody microinjection reveals an essential role for human polo-like kinase 1 (Plk1) in the functional maturation of mitotic centrosomes. *J. Cell Biol.* 135:1701–1713. <https://doi.org/10.1083/jcb.135.6.1701>
- Lee, K., and K. Rhee. 2011. PLK1 phosphorylation of pericentrin initiates centrosome maturation at the onset of mitosis. *J. Cell Biol.* 195:1093–1101. <https://doi.org/10.1083/jcb.201106093>
- Legrand-Poels, S., G. Kustermaans, F. Bex, E. Kremmer, T.A. Kufer, and J. Piette. 2007. Modulation of Nod2-dependent NF- κ B signaling by the actin cytoskeleton. *J. Cell Sci.* 120:1299–1310. <https://doi.org/10.1242/jcs.03424>
- Lou, Y., J. Yao, A. Zereshki, Z. Dou, K. Ahmed, H. Wang, J. Hu, Y. Wang, and X. Yao. 2004. NEK2A interacts with MAD1 and possibly functions as a novel integrator of the spindle checkpoint signaling. *J. Biol. Chem.* 279:20049–20057. <https://doi.org/10.1074/jbc.M314205200>
- Magidson, V., C.B. O'Connell, J. Loncarek, R. Paul, A. Mogilner, and A. Khodjakov. 2011. The spatial arrangement of chromosomes during prometaphase facilitates spindle assembly. *Cell.* 146:555–567. <https://doi.org/10.1016/j.cell.2011.07.012>
- Mardin, B.R., and E. Schiebel. 2012. Breaking the ties that bind: new advances in centrosome biology. *J. Cell Biol.* 197:11–18. <https://doi.org/10.1083/jcb.201108006>
- Mardin, B.R., C. Lange, J.E. Baxter, T. Hardy, S.R. Scholz, A.M. Fry, and E. Schiebel. 2010. Components of the Hippo pathway cooperate with Nek2 kinase to regulate centrosome disjunction. *Nat. Cell Biol.* 12:1166–1176. <https://doi.org/10.1038/ncb2120>
- Mardin, B.R., F.G. Agircan, C. Lange, and E. Schiebel. 2011. Plk1 controls the Nek2A-PP1 γ antagonism in centrosome disjunction. *Curr. Biol.* 21:1145–1151. <https://doi.org/10.1016/j.cub.2011.05.047>
- Mardin, B.R., M. Isokane, M.R. Cosenza, A. Krämer, J. Ellenberg, A.M. Fry, and E. Schiebel. 2013. EGF-induced centrosome separation promotes mitotic progression and cell survival. *Dev. Cell.* 25:229–240. <https://doi.org/10.1016/j.devcel.2013.03.012>
- McHedlishvili, N., S. Wieser, R. Holtackers, J. Mouysset, M. Belwal, A.C. Amaro, and P. Meraldi. 2012. Kinetochores accelerate centrosome separation to ensure faithful chromosome segregation. *J. Cell Sci.* 125:906–918. <https://doi.org/10.1242/jcs.091967>
- Nam, H.J., and J.M. van Deursen. 2014. Cyclin B2 and p53 control proper timing of centrosome separation. *Nat. Cell Biol.* 16:538–549. <https://doi.org/10.1038/ncb2952>
- Naro, C., F. Barbagallo, P. Chieffi, C.F. Bourgeois, M.P. Paronetto, and C. Sette. 2014. The centrosomal kinase NEK2 is a novel splicing factor kinase involved in cell survival. *Nucleic Acids Res.* 42:3218–3227. <https://doi.org/10.1093/nar/gkt1307>
- Nigg, E.A., and T. Stearns. 2011. The centrosome cycle: Centriole biogenesis, duplication and inherent asymmetries. *Nat. Cell Biol.* 13:1154–1160. <https://doi.org/10.1038/ncb2345>
- Obino, D., F. Farina, O. Malbec, P.J. Sáez, M. Maurin, J. Gaillard, F. Dingli, D. Loew, A. Gautreau, M.-I. Yuseff, et al. 2016. Actin nucleation at the centrosome controls lymphocyte polarity. *Nat. Commun.* 7:10969. <https://doi.org/10.1038/ncomms10969>

- Palazzo, R.E., J.M. Vogel, B.J. Schnackenberg, D.R. Hull, and X. Wu. 2000. Centrosome maturation. *Curr. Top. Dev. Biol.* 49:449–470. [https://doi.org/10.1016/S0070-2153\(99\)49021-0](https://doi.org/10.1016/S0070-2153(99)49021-0)
- Prosser, S.L., N.K. Sahota, L. Pelletier, C.G. Morrison, and A.M. Fry. 2015. Nek5 promotes centrosome integrity in interphase and loss of centrosome cohesion in mitosis. *J. Cell Biol.* 209:339–348. <https://doi.org/10.1083/jcb.201412099>
- Ran, F.A., P.D. Hsu, J. Wright, V. Agarwala, D.A. Scott, and F. Zhang. 2013. Genome engineering using the CRISPR-Cas9 system. *Nat. Protoc.* 8: 2281–2308. <https://doi.org/10.1038/nprot.2013.143>
- Rellos, P., F.J. Ivins, J.E. Baxter, A. Pike, T.J. Nott, D.-M. Parkinson, S. Das, S. Howell, O. Fedorov, Q.Y. Shen, et al. 2007. Structure and regulation of the human Nek2 centrosomal kinase. *J. Biol. Chem.* 282:6833–6842. <https://doi.org/10.1074/jbc.M609721200>
- Sawin, K.E., K. LeGuellec, M. Philippe, and T.J. Mitchison. 1992. Mitotic spindle organization by a plus-end-directed microtubule motor. *Nature.* 359:540–543. <https://doi.org/10.1038/359540a0>
- Schindelin, J., I. Arganda-Carreras, E. Frise, V. Kaynig, M. Longair, T. Pietzsch, S. Preibisch, C. Rueden, S. Saalfeld, B. Schmid, et al. 2012. Fiji: an open-source platform for biological-image analysis. *Nat. Methods.* 9: 676–682. <https://doi.org/10.1038/nmeth.2019>
- Shen, Y., P. Liu, T. Jiang, Y. Hu, F.K.C. Au, and R.Z. Qi. 2017. The catalytic subunit of DNA polymerase δ inhibits γ TuRC activity and regulates Golgi-derived microtubules. *Nat. Commun.* 8:554. <https://doi.org/10.1038/s41467-017-00694-2>
- Silkworth, W.T., and D. Cimini. 2012. Transient defects of mitotic spindle geometry and chromosome segregation errors. *Cell Div.* 7:19. <https://doi.org/10.1186/1747-1028-7-19>
- Silkworth, W.T., I.K. Nardi, R. Paul, A. Mogilner, and D. Cimini. 2012. Timing of centrosome separation is important for accurate chromosome segregation. *Mol. Biol. Cell.* 23:401–411. <https://doi.org/10.1091/mbc.e11-02-0095>
- Smith, E., N. Hégarat, C. Vesely, I. Roseboom, C. Larch, H. Streicher, K. Straatman, H. Flynn, M. Skehel, T. Hirota, et al. 2011. Differential control of Eg5-dependent centrosome separation by Plk1 and Cdk1. *EMBO J.* 30:2233–2245. <https://doi.org/10.1038/emboj.2011.120>
- Stroud, M.J., R.A. Kammerer, and C. Ballestrem. 2011. Characterization of G2L3 (GAS2-like 3), a new microtubule- and actin-binding protein related to spectraplakins. *J. Biol. Chem.* 286:24987–24995. <https://doi.org/10.1074/jbc.M111.242263>
- Stroud, M.J., A. Nazgiewicz, E.A. McKenzie, Y. Wang, R.A. Kammerer, and C. Ballestrem. 2014. GAS2-like proteins mediate communication between microtubules and actin through interactions with end-binding proteins. *J. Cell Sci.* 127:2672–2682. <https://doi.org/10.1242/jcs.140558>
- Suozi, K.C., X. Wu, and E. Fuchs. 2012. Spectraplakins: master orchestrators of cytoskeletal dynamics. *J. Cell Biol.* 197:465–475. <https://doi.org/10.1083/jcb.201112034>
- Tang, D.D., and S.J. Gunst. 2004. The small GTPase Cdc42 regulates actin polymerization and tension development during contractile stimulation of smooth muscle. *J. Biol. Chem.* 279:51722–51728. <https://doi.org/10.1074/jbc.M408351200>
- Toso, A., J.R. Winter, A.J. Garrod, A.C. Amaro, P. Meraldi, and A.D. McAinsh. 2009. Kinetochore-generated pushing forces separate centrosomes during bipolar spindle assembly. *J. Cell Biol.* 184:365–372. <https://doi.org/10.1083/jcb.200809055>
- Uto, K., and N. Sagata. 2000. Nek2B, a novel maternal form of Nek2 kinase, is essential for the assembly or maintenance of centrosomes in early *Xenopus* embryos. *EMBO J.* 19:1816–1826. <https://doi.org/10.1093/emboj/19.8.1816>
- Uzbekov, R., I. Kireyev, and C. Prigent. 2002. Centrosome separation: respective role of microtubules and actin filaments. *Biol. Cell.* 94:275–288. [https://doi.org/10.1016/S0248-4900\(02\)01202-9](https://doi.org/10.1016/S0248-4900(02)01202-9)
- Vaughan, S., and H.R. Dawe. 2011. Common themes in centriole and centrosome movements. *Trends Cell Biol.* 21:57–66. <https://doi.org/10.1016/j.tcb.2010.09.004>
- Vlijm, R., X. Li, M. Panic, D. Rüttnick, S. Hata, F. Herrmannsdörfer, T. Kuner, M. Heilemann, J. Engelhardt, S.W. Hell, and E. Schiebel. 2018. STED nanoscopy of the centrosome linker reveals a CEP68-organized, periodic rootletin network anchored to a C-Nap1 ring at centrioles. *Proc. Natl. Acad. Sci. USA.* 115:E2246–E2253. <https://doi.org/10.1073/pnas.1716840115>
- Wang, W., L. Chen, Y. Ding, J. Jin, and K. Liao. 2008. Centrosome separation driven by actin-microfilaments during mitosis is mediated by centrosome-associated tyrosine-phosphorylated cortactin. *J. Cell Sci.* 121:1334–1343. <https://doi.org/10.1242/jcs.018176>
- Wolter, P., K. Schmitt, M. Fackler, H. Kremling, L. Probst, S. Hauser, O.J. Gruss, and S. Gaubatz. 2012. GAS2L3, a target gene of the DREAM complex, is required for proper cytokinesis and genomic stability. *J. Cell Sci.* 125:2393–2406. <https://doi.org/10.1242/jcs.097253>
- Yang, J., M. Adamian, and T. Li. 2006. Rootletin interacts with C-Nap1 and may function as a physical linker between the pair of centrioles/basal bodies in cells. *Mol. Biol. Cell.* 17:1033–1040. <https://doi.org/10.1091/mbc.e05-10-0943>
- Zhang, Y., O. Foreman, D.A. Wigle, F. Kosari, G. Vasmatzis, J.L. Salisbury, J. van Deursen, and P.J. Galardy. 2012. USP44 regulates centrosome positioning to prevent aneuploidy and suppress tumorigenesis. *J. Clin. Invest.* 122:4362–4374. <https://doi.org/10.1172/JCI63084>

Supplemental material

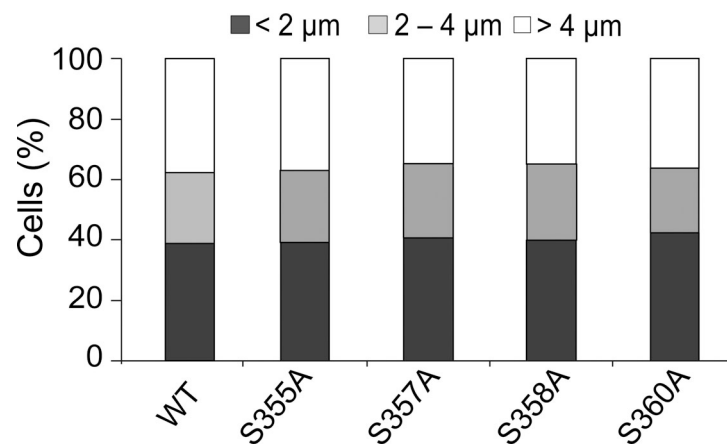


Figure S1. **Ser-to-Ala substitution at position 355, 357, 358, or 360 does not affect centrosome-separating activity of GAS2L1.** RPE-1 cells were transfected with GFP-tagged GAS2L1 WT or mutants (S355A, S357A, S358A, and S360A), and stained with an anti- γ -tubulin antibody. Centrosome distance was measured from three independent experiments: $n = 110$ (WT), 114 (S355A), 121 (S357A), 98 (S358A), and 104 (S360A).

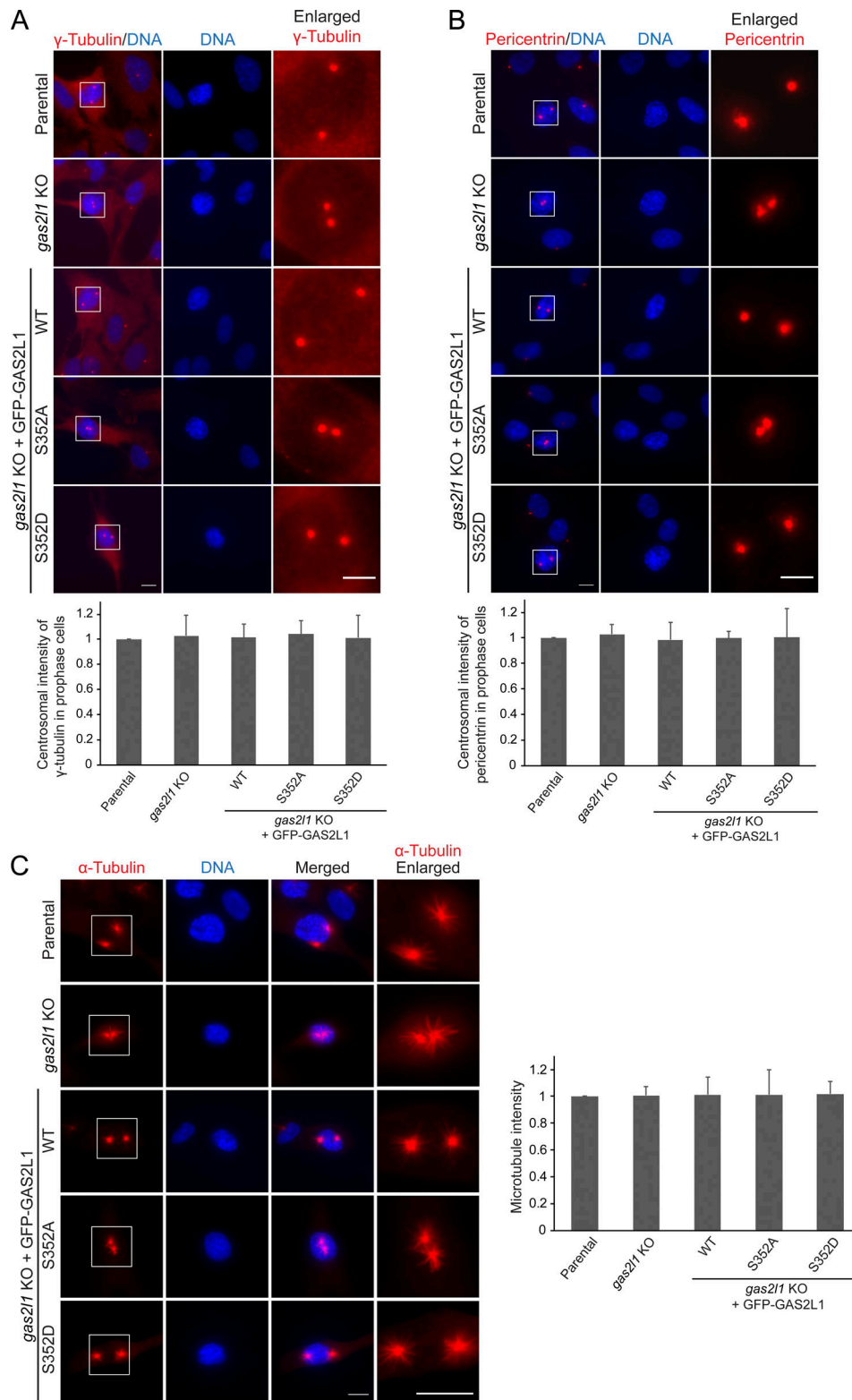


Figure S2. ***gas2l1* knockout or the disruption of GAS2L1 Ser352 phosphorylation does not affect centrosome maturation. (A and B)** RPE-1 parental cells and sublines were stained for (A) γ -tubulin or (B) pericentrin. DNA was labeled with Hoechst 33258. Prophase cells were identified based on DNA patterns and analyzed for centrosomal intensities of γ -tubulin and pericentrin; data were collected from three independent experiments. Arrowheads: centrosomes. γ -Tubulin: $n = 52$ (Parental), 58 (*gas2l1* KO), 61 (*gas2l1* KO + WT), 55 (*gas2l1* KO + S352A), and 50 (*gas2l1* KO + S352D). Pericentrin: $n = 48$ (Parental), 51 (*gas2l1* KO), 44 (*gas2l1* KO + WT), 49 (*gas2l1* KO + S352A), and 56 (*gas2l1* KO + S352D). **(C)** Microtubule regrowth assay was performed on RPE-1 parental cells and sublines. Microtubules were visualized through anti- α -tubulin labeling, and DNA was stained with Hoechst 33258. Centrosome-based microtubule asters were quantified in prophase cells from three independent experiments: $n = 50$ (Parental), 50 (*gas2l1* KO), 51 (*gas2l1* KO + WT), 55 (*gas2l1* KO + S352A), and 53 (*gas2l1* KO + S352D). Boxed regions are enlarged to show microtubule asters. Scale bars, 10 μ m.

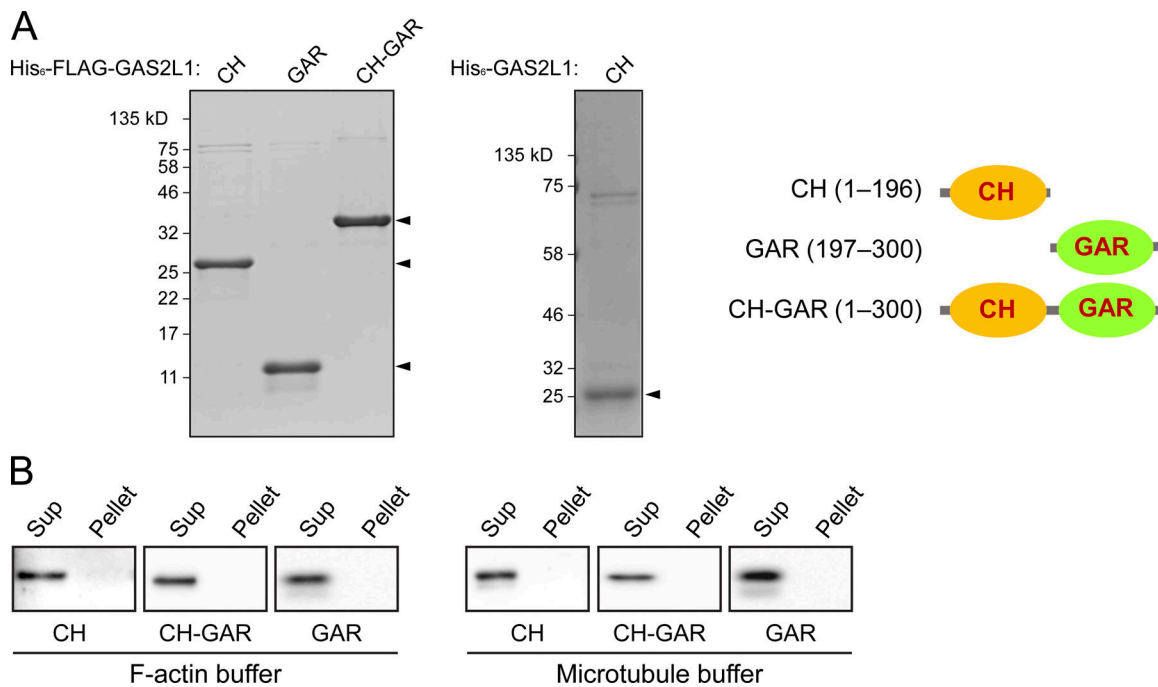


Figure S3. **Analysis of purified bacterially expressed GAS2L1 fragments.** (A) GAS2L1 fragments harboring a His₆-FLAG or His₆ tag were expressed in bacteria and purified through the His₆ tag. Purified proteins were analyzed using SDS-PAGE and Coomassie Blue staining. Arrowheads: recombinant proteins. (B) Recombinant GAS2L1 fragments (His₆-tagged) were used in F-actin or microtubule sedimentation assays in the absence of F-actin or microtubules, respectively, in actin polymerization buffer (F-actin buffer) or BRB80 buffer (microtubule buffer). Pellets and supernatants were collected after sedimentation for anti-His₆ immunoblotting.

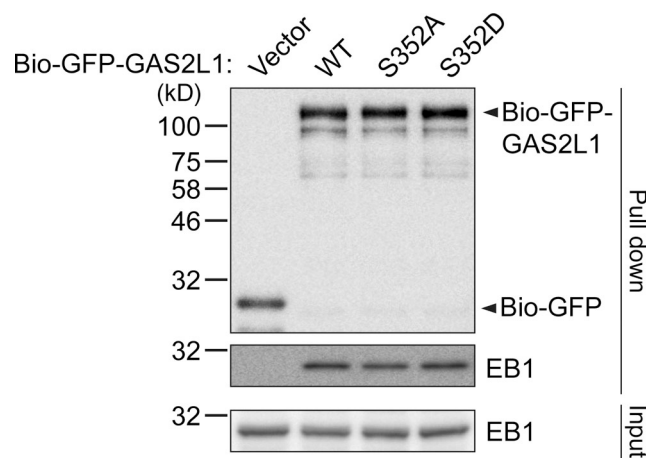


Figure S4. **Binding of Ser352 mutants of GAS2L1 to EB1.** Bio-GFP-tagged GAS2L1 constructs were transiently expressed in HEK293T cells and pulled down using streptavidin beads. Aliquots of the pull-downs (50%) and lysate inputs (2%) were immunoblotted for GFP and EB1. WT, GAS2L1 WT.

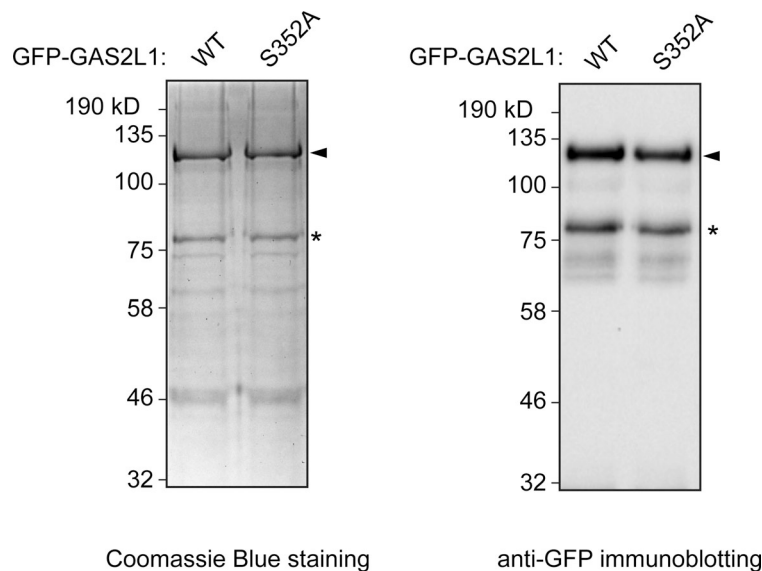


Figure S5. **GAS2L1 and its S352A mutant prepared from HEK293T cells expressing the proteins.** GFP-tagged GAS2L1 WT and S352A mutant, both also containing a biotinylation tag, were expressed in HEK293T cells, purified using streptavidin-coupled beads, resolved on SDS-PAGE gels, and analyzed through Coomassie Blue staining and anti-GFP immunoblotting. Arrowheads: GFP-GAS2L1 full-length protein; asterisks: fragment of the protein.

Video 1. **Centrosome movement in parental RPE-1 cells in late G2 and mitosis.** Time-lapse image sequences were taken at 8-min intervals. Microtubules and centrosomes were visualized using SiR-tubulin, and DNA was visualized with Hoechst 33342. Video corresponds to Fig. 3 A. Frame rate of the video is 3 frames per second.

Video 2. **Centrosome movement in *gas2l1*^{-/-} RPE-1 cells in late G2 and mitosis.** Time-lapse image sequences were taken at 8-min intervals. Microtubules and centrosomes were visualized using SiR-tubulin, and DNA was visualized with Hoechst 33342. Video corresponds to Fig. 3 A. Frame rate of the video is 3 frames per second.

Video 3. **Centrosome movement in *gas2l1*^{-/-} RPE-1 cells expressing GFP-GAS2L1 in late G2 and mitosis.** Time-lapse image sequences were taken at 8-min intervals. Microtubules and centrosomes were visualized using SiR-tubulin, and DNA was visualized with Hoechst 33342. Video corresponds to Fig. 3 A. Frame rate of the video is 3 frames per second.

Video 4. **Centrosome movement in *gas2l1*^{-/-} RPE-1 cells expressing the S352A mutant of GFP-GAS2L1 in late G2 and mitosis.** Time-lapse image sequences were taken at 8-min intervals. Microtubules and centrosomes were visualized using SiR-tubulin, and DNA was visualized with Hoechst 33342. Video corresponds to Fig. 3 A. Frame rate of the video is 3 frames per second.

Video 5. **Centrosome movement in *gas2l1*^{-/-} RPE-1 cells expressing the S352D mutant of GFP-GAS2L1 in late G2 and mitosis.** Time-lapse image sequences were taken at 8-min intervals. Microtubules and centrosomes were visualized using SiR-tubulin, and DNA was visualized with Hoechst 33342. Video corresponds to Fig. 3 A. Frame rate of the video is 3 frames per second.